Review of Materials Research 1 (2025) 100006

Contents lists available at ScienceDirect

Review of Materials Research

journal homepage: www.sciencedirect.com/journal/review-of-materials-research

Microstructure control on optimizing energy storage performance for dielectric ceramic

Minhao Zhang, Jinquan Zeng, Yiying Chen, Shun Lan, Yan Song, Yuanhua Lin *

State Key Laboratory of New Ceramics and Fine Processing, School of Materials Science and Engineering, Tsinghua University, Beijing, 100084, China

ARTICLE INFO

Keywords:
Microstructure
Dielectric ceramic
Energy storage
Microstructure-performance relationship

ABSTRACT

This review focuses on recent progress in optimizing the energy storage performance of dielectric ceramic and indicates the correlation between performance and the designed microstructure. Principles and key parameters of dielectric energy storage are described, and optimized strategies on microstructure with improving energy storage performance are briefly collected, named domain engineering, grain refining strategy, textured ceramic design, multi-phase engineering, core-shell structure design, and multilayer structural design. Conclusion with existing challenges and perspectives of microstructure control on optimizing energy storage performance dielectric ceramic are finally presented.

1. Introduction

In recent decades, the continuous development of global economics has raised demands for energy resulting in deterioration of energy crisis, while the related pollution led to growth in environmental awareness of society [1–3]. In this case, the development of sustainable clean energy and high-performance energy storage devices with high efficiency is urgently required [4,5]. Compared to existing electrochemical devices of batteries or supercapacitors that store energy through electrochemical reactions, dielectric capacitors can store energy through accumulation of induced charge by dipole polarization under an external electric field. Such an energy storage mode has ultrafast charge/discharge capability (ns to μs) and large power density (up to MW/m^3), which has attracted growing attention due to its widespread potential applications in modern electronic and electrical devices, especially necessitated in pulse power systems. Mainly so far, dielectric capacitors have been enabled in broad utilization scenarios such as medical apparatus, pulsed lasers, hybrid electric vehicles, flash tubes, military equipment, and aerospace systems [4]. However, the energy density of dielectrics is normally several orders of magnitude lower than that of electrochemical energy stored components, making them difficult used for large-scale energy storage and dissatisfy the increasing requirement for miniaturization. Herein, dielectric materials with higher energy density and efficiency are one of the challenges of current research and are urgently desirable.

In existing work on exploring high energy-storage performance dielectrics, the main types of materials include ceramics [6–10], polymers [11–15], and nanocomposites [16–20], where polymer-based materials are more commonly used in commercial applications due to their high breakdown strength and excellent processability. Nevertheless, low energy density, as well as poor thermal stability resulting from the existence of transition temperature and severe thermal breakdown, makes polymer-based dielectrics difficult applied in serval areas, especially in harsh environments with high operating temperatures. For example, commercial-used dielectric polymer biaxially oriented polypropylene (BOPP) usually has limited energy density to be lower than 2 J/cm^3, and can only maintain undegraded well dielectric performances under 85 °C [21]. In contrast, dielectric ceramics are somewhere relatively advantageous, as they have comparatively high permittivity, good chemical, temperature, and cycling stabilities on multiple or harsh applications with good endurance. Indeed, over 3 trillion multilayer ceramic capacitors (MLCCs) have been fabricated each year mostly using typical dielectric ceramics $BaTiO_3$ (BT) as material, showing wide demands for dielectric ceramics [22,23].

In recent decades of research, the dielectric microstructure is regularly associated with its energy storage performance and has been proven as an influential factor for optimizing energy storage performance. Generally, the microstructure in different scale sizes has specific effects on key parameters of energy storage properties, like breakdown, efficiency, or polarization. For example, in inorganic ceramic systems, macroscopic ferroelectric domains can be broken into nanoscale domains that have much lower switching barriers and thus a slim hysteresis loss, leading to higher efficiency and recoverable energy density. On a larger

* Corresponding author.
E-mail address: linyh@tsinghua.edu.cn (Y. Lin).

https://doi.org/10.1016/j.revmat.2025.100006
Received 23 March 2025; Received in revised form 2 April 2025; Accepted 3 April 2025
Available online 8 April 2025

scale, the parameters of grains have demonstrated a strong impact on energy storage performance. Fined grains or grains with specific textures can exhibit higher breakdown strength, and result in the enhancement of energy density. Moreover, the introduction of secondary phases and accurately controlling the forms of existence are some of the available methods to improve energy density. In mesoscopic scale, lamination of different dielectrics and design of interlayers are proven to be effective methods to combine the advantages of different dielectrics and can achieve optimized energy storage performances (see Table 1). Even though dielectric ceramics can be hierarchically optimized in different scales of microstructure, clarification, as well as deconstruction on related theory and underlying mechanisms, is still insufficient. Briefly, microstructure design at different scales needs to be further recognized, explained, utilized, and combined to promote the development of dielectric for better energy storage properties.

In this review, we first briefly introduce the principles and key parameters of energy storage performance on dielectrics. Typical designs of microstructure that are applied on energy storage dielectric ceramics are collected and summarized, with a brief introduction of the background. More specifically, recent progress on dielectric ceramics is organized into its optimization strategy on microstructure and energy storage performance in the order of certain scales, named domain engineering, grain refining strategy, textured ceramic design, multi-phase engineering, core-shell structure design, and multilayer structural design (see Fig. 1). Finally, a conclusion with existing challenges and perspectives of microstructure effect on dielectric ceramic. Overall, this review aims to point out the significance of microstructure in optimizing energy storage dielectric ceramics and to improve the understanding of microstructure design in different observation scales.

2. Principle and key parameter for energy storage

The simplest parallel plate capacitor has two parallel electrode plates with an inside dielectric layer. Under an external electric field, dipoles in dielectric with random alignment turn elongated and align along the direction of the applied electric field, and charges are accumulated on both conductive sides. Therefore, electrostatic energy can be stored and the value can be determined by the integral of recoverable energy density,

$$W_{rec} = \int_{P_r}^{P_m} E \, dP,$$

where P_m , P_r, and E are the maximum polarization, remnant polarization, and electric field, respectively. The energy efficiency can be expressed as

$$\eta = \frac{W_{rec}}{W_{rec} + W_{loss}},$$

where W_{loss} is partial energy loss caused by the non-coincide of *P-E* loop during charge/discharge process resulting from ferroelectric, conduction, or heat loss. High energy storage dielectrics need to have high recoverable energy density, whereas the intercouple of key parameters including polarizability and breakdown strength E_b makes the optimization of dielectrics energy storage always the process of tradeoff.

According to the domain structures and polarization behaviors, dielectrics can be classified into four categories, normally named as linear dielectric, ferroelectric, antiferroelectric, and relaxor ferroelectric, as shown in Fig. 2. For linear dielectric where relative permittivity ε_r is independent of E, the energy density can be written as

$$W_{rec} = \frac{1}{2}\varepsilon_0 \varepsilon_r E_b^{\,2},$$

where ε_0 is the vacuum permittivity. Linear-like *P–E* characteristics lead to a negligible dielectric loss, with almost full efficiency. However, limited energy density caused by low permittivity restricts further applications. Nevertheless, such dielectric still attracts considerable attention, as it generally possesses a high breakdown strength. Ferroelectric with macroscopic domains has large remnant polarization due to the presence of apparent switching hysteresis under an external electric field. In this case, Ferroelectric is unable to achieve prime energy density with high efficiency. In contrast, relaxor ferroelectric is differentiated from ferroelectric, since it has diffusion phase transition without distinguishable curie temperature. Remanent polarization of relaxor ferroelectric is effectively minimized through chemical modification like doping or forming solid solution [30–32]. Breaking of macroscopic domains into nano-scale domains that have much lower switching barriers leads to a greatly improved efficiency and makes relaxor ferroelectric a promising candidate in energy storage research. Another type of widespread concern on energy storage is antiferroelectric, which has delayed but considerable saturated polarization and near-zero remanent polarization. However, the presence of electric field-induced phase transition leads to the instability of antiferroelectricity and considerable loss, which is one of the main challenges during the optimization of antiferroelectric energy storage performance [33,34].

Table 1
Energy storage performances of dielectrics from representative literature with as-mentioned microstructure control strategies.

Materials	Optimization Strategies	Energy Density (J/cm^3)	Efficiency (%)	Reference
BT-based	Domain engineering	20.8	97.5	24
$K_{0.2}Na_{0.8}NbO_3$-based	Domain engineering	10.06	90.8	6
BT-based	Grain refining strategy	10	–	73
BNT-based	Textured ceramic design	21.5	~80	26
BNT-based	Multi-phase engineering	14.9	93.4	27
Tungsten bronze -based	Multi-phase engineering	12.2	89.5	83
NN-based	Core-shell structure design	7.7	83.8	97
$BiFeO_3$-based	Core-shell structure design	12.1	86.1	98
BNKSTT/BNT–SNA	Multilayer structural design	6.8	89.8	101
BT-based	Multiple strategies	18.2	94.5	105

3. Domain engineering

Domain engineering is a common way to improve performance of dielectric materials for energy storage capacitors. In general, domain engineering aims to lower the switching barriers of domains. Because of high Landau energy barriers in ferroelectrics, their domains are hard to switch under electric field, showing a rectangle-like hysteresis loop and poor efficiency. Transforming the double-deep-well Landau free energy into shallow-well free energy or splitting a high energy barrier into low energy barriers can effectively enhance the energy storage density of the materials. As a result, the energy density and efficiency are improved.

The basic approach of this strategy is to break long-range ferroelectric domains into discrete polar nanoregions (PNRs) embedded within a non-polar matrix. These regions have relatively low coupling with each other and lower energy barriers, making it easier to overcome the barriers and to achieve switching. Generally, researchers combine ferroelectrics with paraelectric or other weakly polar materials to achieve this goal. Over the past decade, BT-based materials and weakly coupled relaxor ferroelectric, leveraging the concept of domain engineering, have been extensively studied to achieve high energy density and efficiency [35–37]. In addition, Liang et al. incorporated $BiMg_{0.5}Hf_{0.5}O_3$ into $NaNbO_3$ to break

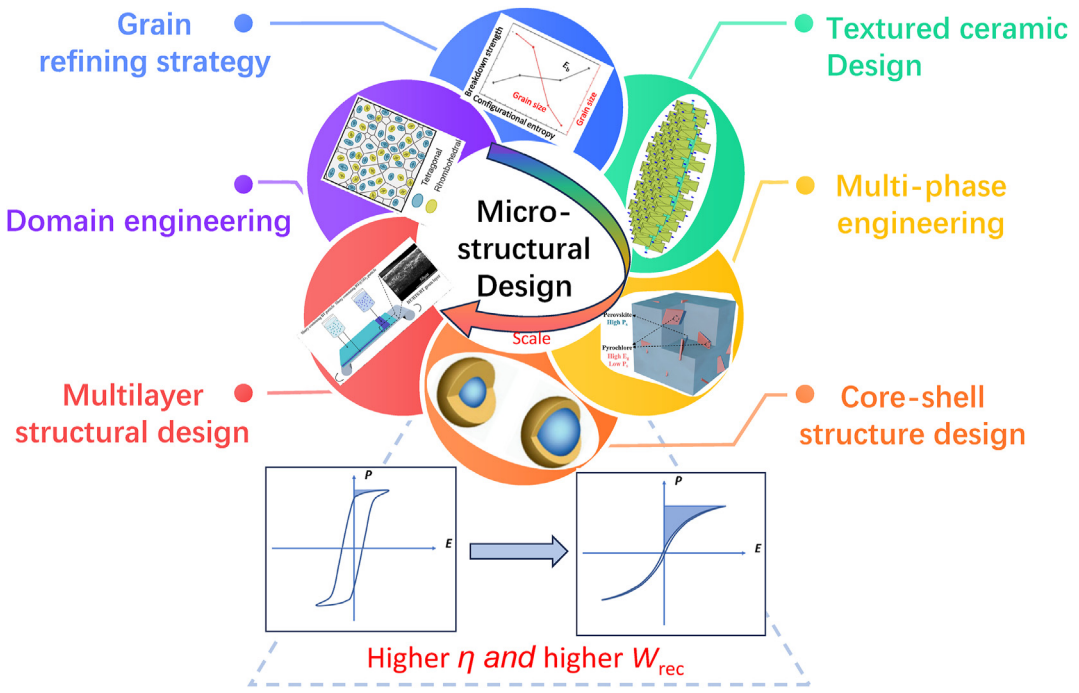

Fig. 1. Schematic diagrams of the optimization strategies on microstructure and energy storage performance in the order of certain scales. The diagram of domain engineering is reproduced from Ref. [24] with permission. The diagram of grain refining strategy is reproduced from Ref. [25] with permission. The diagram of textured ceramic design is reproduced from Ref. [26] with permission. The diagram of multi-phase engineering is reproduced from Ref. [27] with permission. The diagram of core-shell structure design is reproduced from Ref. [28] with permission. The diagram of multilayer structural design is reproduced with permission from Ref. [29] with permission.

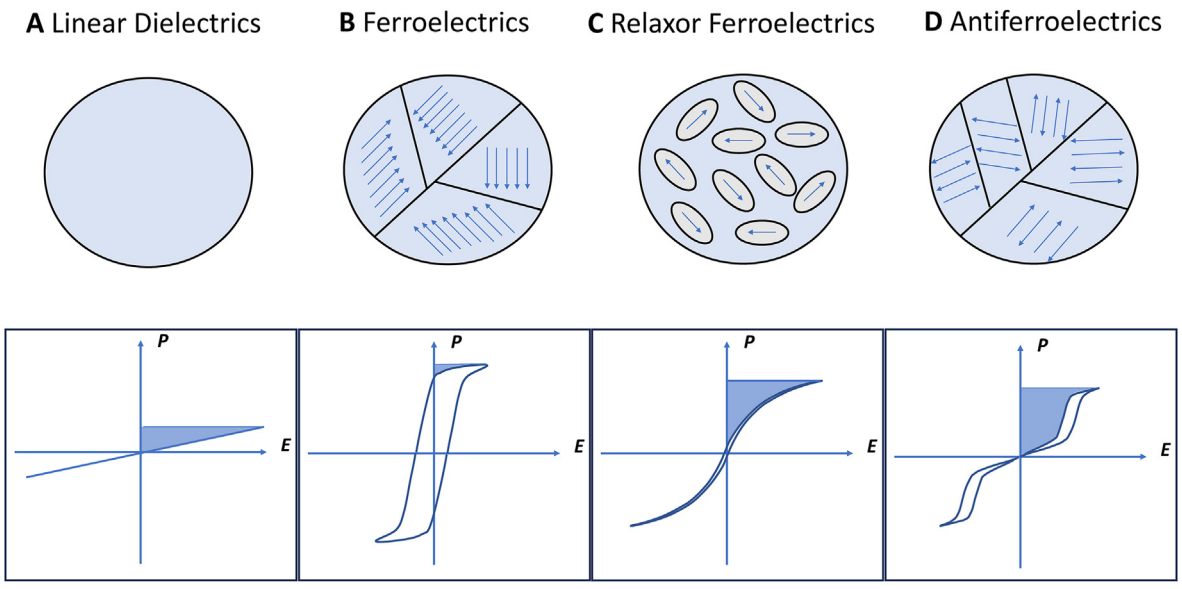

Fig. 2. Schematic illustration of 4 typical types of dielectrics: (A) linear dielectric, (B) ferroelectric, (C) relaxor ferroelectric, (D) antiferroelectric, where the blue shaded areas represent to the recoverable energy density.

the domain structure [38]. This modification effectively enhanced the relaxor behavior as well as enhanced domain switching capability. With larger band gap that improves the E_b, a high energy density of 5.00 J/cm^3 with an efficiency of 83.1 % was obtained. Thong et al. proposed mesoscopic chemical inhomogeneity to design domain structures in $(K_{0.5}Na_{0.5})NbO_3$(KNN) ferroelectric ceramics with fixed chemical stoichiometry [39]. This approach successfully disrupted the long-range domain continuity, reduced domain size, and increased domain wall density. Lv et al. explored $NaNbO_3$–$(Bi_{0.5}Na_{0.5})TiO_3$–$Bi(Mg_{0.5}Hf_{0.5})O_3$ MLCC with an excellent energy density of 12.65 J/cm^3 and an efficiency of 88.5 %, as shown in Fig. 3A [40]. Through disordered tilting around the c_p axis, long-range displacements of Na^+ and Bi^{3+} ions were disrupted, resulting in the induction of PNRs and enhancing relaxor behavior, thus achieving a superior energy storage performance. Zheng et al. broke the long-range-ordered ferroelectric domains by doping Sm^{3+} in A sites and Mg^{2+}/Nb^{5+} in B sites to achieve high excellent RFE properties in $Na_{0.5}Bi_{0.5}TiO_3$ ceramic (Fig. 3B) [41]. Such dopants also resulted in reducing grain sizes, larger band gaps, and creating a highly

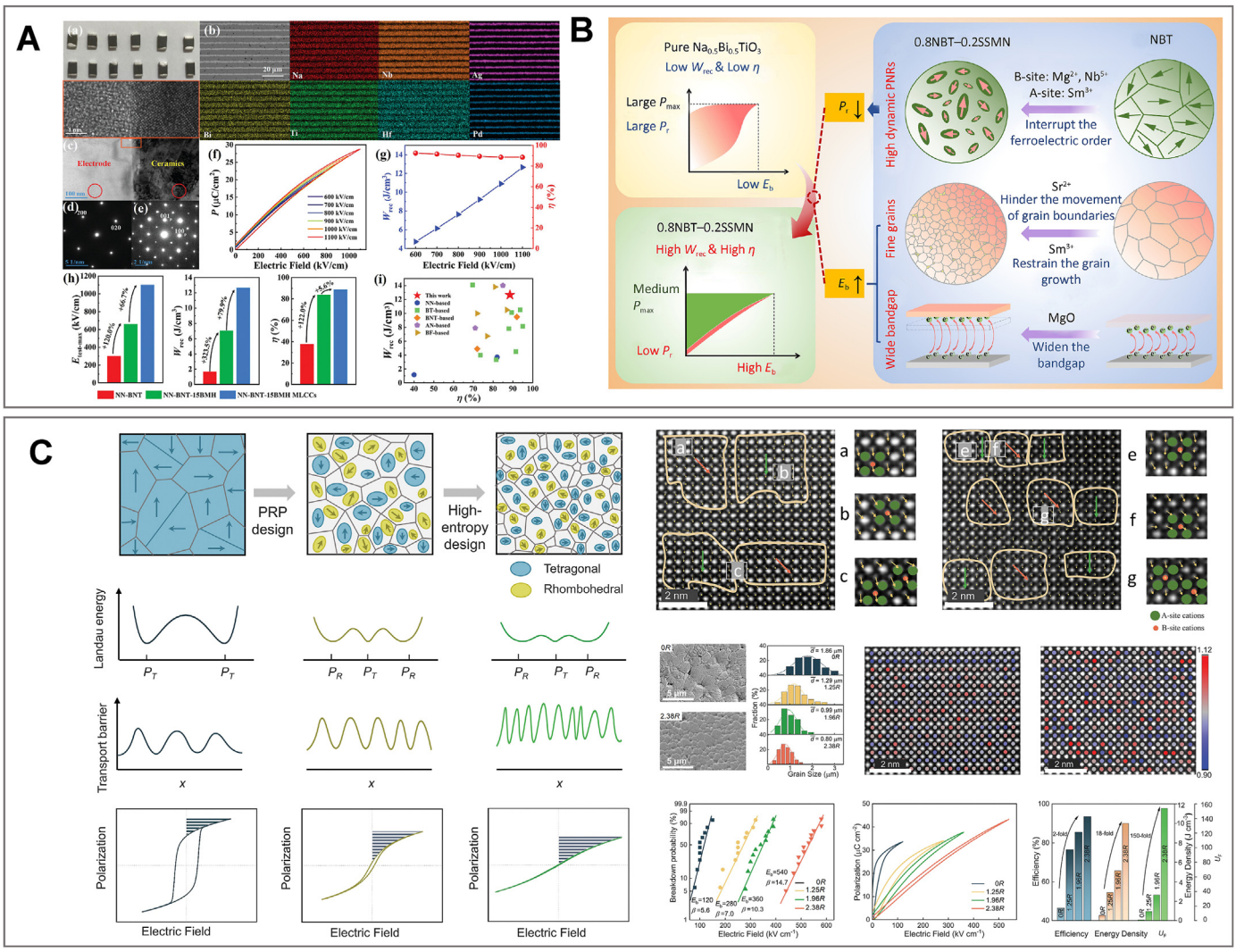

Fig. 3. (A) Schematic diagram of the MLCC with its images and energy storage performance. Reproduced from Ref. [40] with permission. (B) Schematic diagrams of the optimizing strategy to improve energy storage performance. Reproduced from Ref. [41] with permission. (C) Schematic diagram of the high-entropy design strategy for ultrahigh energy storage with polymorphic relaxor phase, images of different phases and displacement of B-site cation in each unit cell, and dielectric properties. Reproduced from Ref. [24] with permission.

insulating second phase. Thus, a large recoverable energy density of 7.3J/cm^3 was achieved, caused by the enhanced E_b and improved RFE property.

Recently, a further strategy has been proposed to introduce nano-domains with different symmetries, called polymorphic domains. In such a system containing multiple variant domains, the Landau energy barrier would be further decreased compared with the single symmetry PNRs. Notably, since ferroelectric components have higher concentration, higher polarization could be maintained in this strategy. Under these conditions, ultra-high energy density and high efficiency can be achieved simultaneously. Jiang et al. utilized domain engineering to fabricate $NaNbO_3$-$BiFeO_3$ bulk ceramics that combine the advantages of both antiferroelectric and relaxor materials, resulting in an energy density of 18.5 J/cm^3 [42]. Zhang et al. proposed a design strategy to enhance the energy storage performance of $BaTi_{0.96}Li_{0.04}O_{2.94}$ ceramics through domain structure engineering [43]. This enhancement was attributed to the creation of a unique crossover region between the ferroelectric and relaxor ferroelectric states that were characterized by ferroelectric domains of varying scales. Zhang et al. proposed the implementation of polymorphic relaxor phases in $BaTiO_3$-based MLCC by strategically incorporating different local symmetries and exhibited an energy density of 20.8 J/cm^3 in MLCC [24]. Such a design effectively decreased the domain-switching barriers that minimized hysteresis loss. High atomic disorder with lattice distortion and grain refining enhanced the breakdown strength, as shown in Fig. 3C. Chen et al. proposed a high-entropy strategy, doping multiple elements to induce rhombohedral-orthorhombic-tetragonal-cubic multiphase nanoclusters and random oxygen octahedral tilt in $K_{0.2}Na_{0.8}NbO_3$ ceramic, resulting in ultrasmall PNRs that enhance E_b and delayed polarization saturation, and achieved a high energy density of 10.06 J/cm^3 [6].

In conclusion, domain engineering has emerged as a powerful approach to optimizing the energy storage performance of dielectric materials. Benefiting from their decreased domain size and enhanced dynamical properties, researchers have reported significantly enhanced overall performance, including energy density, efficiency, and reliability in many systems. These advancements not only deepen our understanding of dielectric behavior but also pave the way for the development of high-performance energy storage systems, meeting the increasing demands of modern electronic and energy applications.

4. Grain refining strategy

Materials with dense microstructure and fine grain size are ideal dielectrics with balanced polarization, high E_b, and high energy storage

density (Fig. 4A and B [5]). The polarization, relaxation behavior, and E_b of dielectric materials are generally impacted by the sintering effect through grain tailoring techniques.

The E_b of ceramics decreases rapidly with increasing porosity and/or density, i.e., dense ceramics with uniform and fine grains have higher E_b. This is because pores or voids with low electrical E_b can lead to premature partial (local) breakdown of the dielectric, causing erosion, electrical treeing, and pitting, which can impair the long-term electrical performance of the dielectric [44]. According to the empirical formula: $E_b \propto (\text{grain size G})^{-a}$ proposed by Tunkasiri, where a is the exponent value being in the range of 0.2–0.4, the E_b is negatively correlated to the grain size [45,46]. This can be explained by the accumulation of depleted space charge layers at the ceramic grain boundaries, leading to high resistivity at the grain boundaries [47]. Grain boundaries create depletion regions that can act as barriers to the transport of charge carriers across the grain boundaries. As the grain size decreases, increased grain boundaries with high resistivity provide more barriers for the transport of charge carriers, resulting in the decrease of the leakage current and the increase of thermal E_b. In the meantime, grain boundaries with higher resistivity can absorb the energy of the electric tree expansion within the grain and prevent electrical breakdown. Decreasing grain size to the submicron scale can also help improve the microscopic electrical homogeneity of the ceramics, reduce short-circuit conduction pathways, and thus improve the E_b. The improvement of the E_b by refining the grain size has been demonstrated by many researchers [48–50]. It has been reported that grain size also affects the dielectric properties of materials [51–54], with both the maximum polarization and the remnant polarization decreasing as the grain size decreases. At the same time, grain refinement can improve the phase transition temperature or relaxation behavior of ceramics. Therefore, high-density fine-grained ceramics may have slim hysteresis loops and high E_b, which is beneficial to improving energy storage performance, including energy density and efficiency. Moreover, it has been reported that the reduction of grain size is positively correlated with the increase in material strength [55,56]. This is because as the grain size decreases, the number of grain boundaries increases, or the segregation phase is formed, which enhances the dislocation-blocking effect and is beneficial to improving the mechanical properties, microstructural stability, and chemical stability of the ceramic.

Various approaches have been proposed to reduce grain size and obtain fine-grained ceramics, including regulating the synthesizing process (sintering conditions and sintering aids), forming special microstructures (second phases and core-shell structures), controlling ion diffusion characteristics (solid solution end members and entropy engineering), etc. The synthesis process has a strong impact on the growth and densification of ceramic particles. Typically, the grain size of ceramics can be reduced to nanoscale by wet-chemical synthesis [43,57,

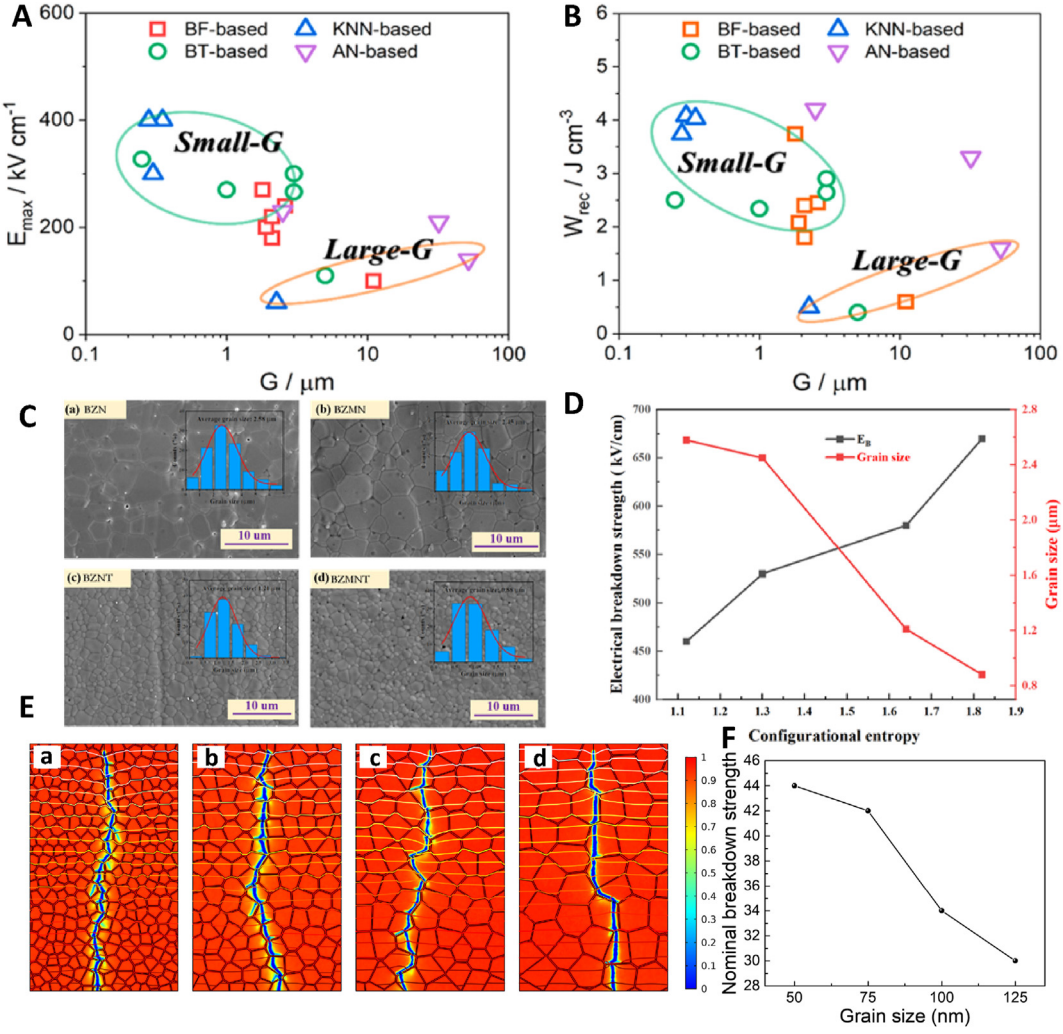

Fig. 4. Relationship between energy storage properties of ceramics and G: (A) G vs E_{max} (E_b), (B) G vs W_{rec}. A and B are reproduced from Ref. [5] with permission. (C) SEM images of (a) BZN, (b) BZMN, (c) BZNT, and (d) BZMNT. (D) Calculated E_b and average grain size as a function of configurational entropy of the four samples. C and D are reproduced from Ref. [25] with permission. (E) Modeled breakdown path of different grain sizes: (a) 50 nm, (b) 75 nm, (c) 100 nm, and (d) 125 nm. (F) The relationship of the modeled nominal E_b vs. grain size. E and F are reproduced from Ref. [44] with permission.

58], high-energy ball milling [55,59,60], spark plasma sintering [61–63], microwave sintering [64–66] and two-step sintering [67–70], to name a few. Wang et al. first proposed a two-step sintering method and then combined it with high-energy ball milling to fabricate $(K_{0.5}Na_{0.5})NbO_3$-$Bi(Zn_{2/3}(Ta_{0.5}Nb_{0.5})_{1/3})O_3$ (KNN-BZTN) relaxor ferroelectric ceramics [59]. As the grain size decreased from 410 nm to 200 nm, the E_b increased nearly 1.5 times from 222 to 317 kV/cm. Yan et al. found that smaller grain size was achieved in TSSM (5 μm in traditional one-step vs. 3.6 μm in two-step sintering method) in $BiFeO_3$-$SrTiO_3$ solid solution, which contributes to a higher energy storage performance (W_{rec} = 8.4 J/cm^3 and η~90 %) [69]. Zhou et al. reported a nanocrystalline $CaTiO_3$ ceramic prepared by the spark plasma sintering method, which showed lower porosity, smaller pore size, and fewer defects and dislocations, and its electrical energy storage density (6.9 J/cm^3) was nearly five-fold than that of the conventional sintered sample (1.5 J/cm^3) [61]. The methods of reducing grain size by fabricating special microstructures and local structure engineering have certain similarities, both of which tailor grain growth by regulating the diffusion characteristics between different ions [24,71,72]. Chen et al. reported a high-entropy design in pyrochlore-structured $Bi_{1.5}Zn_{0.75}Mg_{0.25}Nb_{0.75}Ta_{0.75}O_7$ ceramics, where a reduced grain size (2.58–0.88 μm) and improved E_b (460–670 kV/cm) were observed (Fig. 4C and D) [25]. Tomozawa et al. constructed a nanoscale core-shell structure by depositing a low-melting-point glass layer on the $BaTiO_3$ nanoparticles. The controllable structure possessed high polarization and high E_b, as well as the highest energy density of ~10 J/cm^3 achieved at 1000 kV/cm [73]. A $Bi(Zn_{2/3}Nb_{1/3})O_3$-$(Bi_{0.5}Na_{0.5})TiO_3$-$BaTiO_3$ ternary ceramic was designed by Zhang et al., where the grain size decreased and distributed uniformly through the introduction of the third end member, resulting in a high energy storage density of 4.23 J/cm^3 [74]. Cai et al. simulated the breakdown path of samples with different grain sizes, and proved that decreasing grain size leads to improved E_b [44] (Fig. 4E and F).

In summary, the realization of high E_b and low loss in ceramics is the basic guarantee for achieving excellent energy storage performance. These balanced properties can be achieved in grain-refined ceramics in a variety of ways. Through fine-grained engineering, ceramics can possess high structural strength, superior energy storage performance, and stability, however, the control of the uniformity of fine grains deserves further consideration.

5. Textured ceramic design

Partial dielectric ceramics present intense anisotropic dielectric properties. For example, in ABO_3 perovskite ceramics, maximum electrostriction is along the crystallographic <100> direction, which is the direction of B–O chains, while the minimum electrostriction is along the <111> direction [75]. Such a characteristic makes the design of texture available to improve the piezoelectric performances. Meanwhile, this method has been proven to be effective in optimizing the energy storage performance of dielectric ceramics in recent years, since it can tune the ferroelectric phase transition or reduce the electric-field-induced strain, conducing to better efficiency and breakdown strength.

In this regard, Bai et al. reported the $0.94Bi_{0.5}Na_{0.5}TiO_3$(BNT)-$0.06BaTiO_3$ solid solution with 79.4 % <00l>-oriented that synthesized through template grain growth (TGG) approach, using antiferroelectric $NaNbO_3$(NN) as the growth template [76]. For a very high strain, small hysteresis was achieved under a low electric field, driving to a high recoverable energy density of 1.6 J/cm^3 under a low electric field of 120 kV/cm. Such a highly oriented microstructure was beneficial to domain switching and mobility, promoting ergodic relaxor to ferroelectric phase

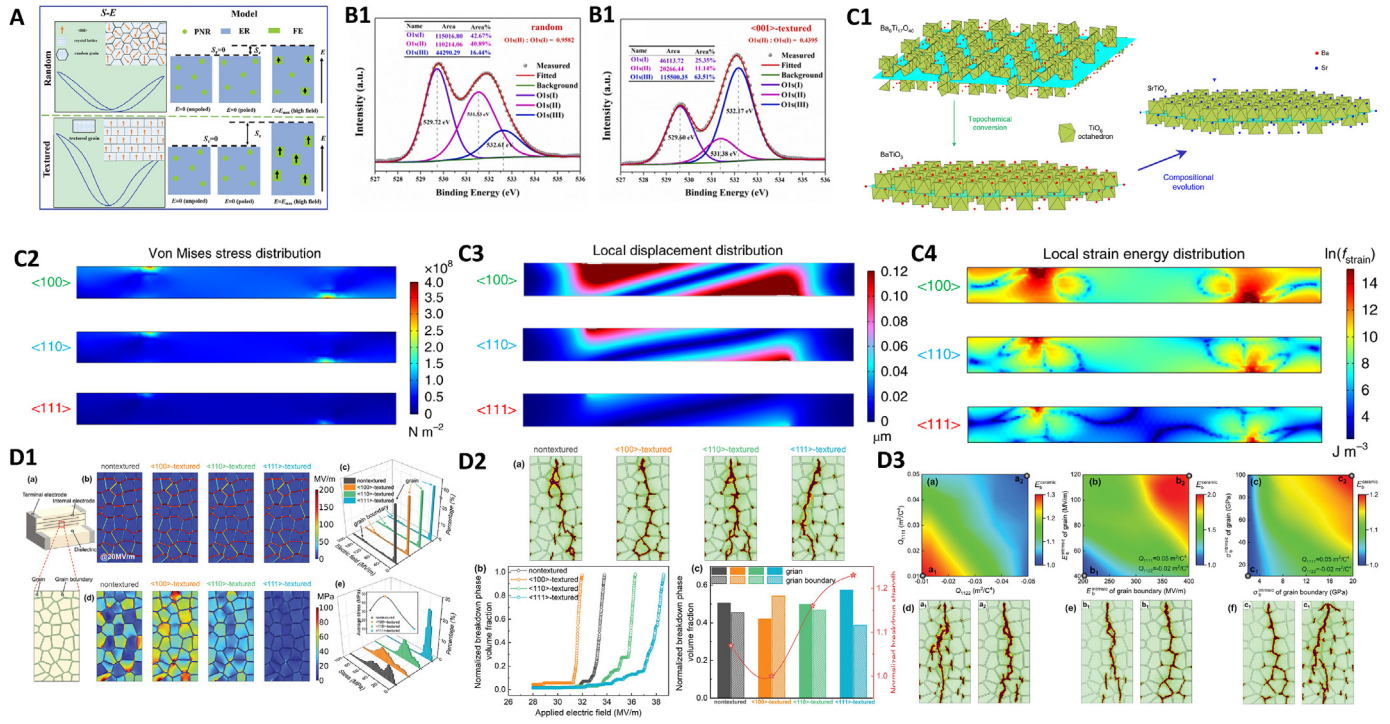

Fig. 5. (A) Mechanism of significantly improved field-induced strain behavior of textured samples compared to random samples. Reproduced from Ref. [76] with permission. (B1, B2). XPS spectra of oxygen elements for textured and non-textured samples, respectively. Reproduced from Ref. [78] with permission. (C1) Schematic of the crystal structure for growth templates. (C2, C3, C4) Local displacements, local distribution of von Mises stresses and local elastic energy densities for <100>−, <110>− and <111>-oriented perovskite samples with applied electric field of 70 MV/m in simulations. Reproduced from Ref. [26] with permission. (D1) The schematic diagram and the selected typical region of MLCC, local distribution of electric field with statistical distributions of local electric field, and local distribution of stress field with statistical distributions of local stress field. (D2) The evolution of electrical trees for different textured ceramic, normalized breakdown phase volume fraction of ceramics vs applied electric field, and comparisons of the normalized breakdown phase volume fraction distribution with the normalized breakdown strength of ceramics, respectively. (D3) High-throughput simulations of E_b depending on different parameters, indicating the evolution of electrical trees at each point. Reproduced from Ref. [80] with permission.

transition and resulting in increasing strain and energy density, the mechanisms are shown in Fig. 5A. Chen et al. reported 70 % orientation degree <001>− textured $Na_{0.7}Bi_{0.1}NbO_3$ ceramic fabricated by the TGG method using ⟨001⟩-oriented $NaNbO_3$ as growth template [77]. Benefiting from the improved interfacial polarization and clamping effect in this textured ceramic, a high recoverable energy density of 2.4 J/cm^3 and efficiency of 85.6 % were achieved.

Ji et al. reported <001>-oriented $0.7(0.99Bi_{0.5}Na_{0.5}TiO_3$-$0.01BiYbO_3)$-$0.3SrTiO_3$(BNT-BY-STO) through TGG method using <001 > -oriented BNT as growth template [78]. The results illustrate that compared to non-textured ceramics, textured ceramics had higher impedance value with less defect, as shown in Fig. 5B1 and B2, and with lower leakage current density. In this case, a high recoverable energy density of 5.34 J/cm^3 with a high efficiency of 83.91 % was achieved. Guo et al. reported <111>-oriented $0.8(0.99Bi_{0.5}Na_{0.5}TiO_3$-$0.1BiYbO_3)$-$0.2SrTiO_3$ (BNT-BY-STO) through the TGG method using <111>-oriented BT as growth template [79]. Compared with non-textured samples, textured samples exhibited enhanced diffuse phase transition behavior and showed a high energy density of 3.26 J/cm^3 with an increasing breakdown strength of 290 kV/cm caused by the reducing electrostriction effect.

Li et al. reported the <111>-textured $Na_{0.5}Bi_{0.5}TiO_3$-$Sr_{0.7}Bi_{0.2}TiO_3$(BNT-SBT) multilayer ceramic capacitors with enhancing breakdown strength of 103 MV/m and large recoverable energy density of 21.5 J/cm^3 [26]. Through finite-element simulation, as shown in Fig. 5C2-C4, they first illustrated that the elastic energy density of the <111>-textured samples was orders of magnitude lower compared to that of the <100>-textured counterpart and electric field at the interface between the dielectric matrix and the pore was much smaller in <111>-textured samples, which can be expected to achieve higher breakdown strength. Therein, <111>-textured $SrTiO_3$ plate-like templates were selected as growth templates, as shown in Fig. 5C1, and <111>-textured BNT-0.35SBT multilayer ceramic capacitors were fabricated with the TGG method and tape casting. The enhancing breakdown strength was achieved by the suppressed electric-field-induced strain that results in reducing the probability of microcrack initiation and crack-driven dielectric breakdown, reducing local electric field around the pores, and reducing the growth rate of partial discharge trees resulting from tensile stress and strain. Such electrostrictive effects on the breakdown behavior of textured ceramics were further discussed by Wang et al. [80]. An electromechanical breakdown model of $Na_{0.5}Bi_{0.5}TiO_3$-$Sr_{0.7}Bi_{0.2}TiO_3$ ceramic was developed, and it illustrates the significant correlation between the breakdown process and local electric/strain energy distributions. In this report, the effect of texture configuration on the distributions of local electric/stress fields and corresponding energy density in ceramics was first studied (Fig. 5D1). Further, the effect of different intrinsic material parameters and extrinsic factors on the electromechanical breakdown process were systematically simulated (Fig. 5D2 and D3). Through machine learning from high-throughput simulations, empirical formulas could be deduced to semi-quantitatively predict the breakdown strength of oriented ceramics. Thus, the effectiveness of orientation for improving breakdown strength and energy storage performance was proven, which was helpful for reasonable textured structure designs to restrain electromechanical breakdown and achieve higher energy density.

In summary, reasonable textured design shows the potential in tunning ferroelectric behavior and increasing the breakdown strength, and can be available in the improvement of energy storage performance. Nevertheless, to obtain ideal oriented ceramic, matched growth templates with appropriate texture should be sought out and fabricated. More theoretical and experimental efforts are still needed in designing oriented ceramics.

6. Multi-phase engineering

Most recently, the design of dual-phase or multi-phase structures has received attention in energy-storage dielectric ceramics. In composite structural materials, tremendous efforts have been made in combining components with different unique properties to decouple the correlation between electrical properties and improve overall performance. For example, by filling nanoplate fillers in the polymer matrix, the trade-off between P_m and E_b dielectrics in polymer composites can be effectively balanced, thereby improving the energy storage performance [81]. This strategy gives researchers inspiration to composite with different phase structures and properties in ceramic bulks.

The formation of multi-phase microstructures can be achieved by artificially designing the composite of different phases or by *in situ* precipitation caused by element volatilization and stoichiometric imbalance during sintering. Due to the different growth conditions among different phases, the second phase plays the role of "pinning effect" when sintering composite ceramics, thereby significantly inhibiting grain growth. Therefore, multiphase structures are generally possessed with small grain size. The reduced grain size and the formation of segregation phases are beneficial to improving the mechanical properties, microstructural stability, and chemical stability of ceramics. Moreover, the second phase is generally distributed at the grain boundaries, which is beneficial to the scattering of electron carriers at the grain boundaries and helps to improve the E_b (Fig. 6A, B, C) [82].

In recent years, tremendous work has been conducted in multiphase design in inorganic dielectric energy storage ceramic bulks. By embedding a paraelectric phase ($Bi_2Ti_2O_7$) with high E_b into a ferroelectric phase ($Sr_{0.7}Bi_{0.2}TiO_3$-$Bi0.5Na_{0.5}TiO_3$) with large polarization, Wang et al. reported a dual-phase strategy in $(Bi_{0.5}Na_{0.5})_{0.65}(Sr_{0.7}Bi_{0.2})_{0.35}$-$Ti_{0.88}Hf_{0.12}O_3$ multilayered capacitors with enhanced energy storage of 14.9 J/cm^3 with an efficiency of up to 93.4 % (Fig. 6D, E, F) [27]. Liu et al. proposed a second-phase segregation strategy by forming a perovskite-type second phase into the interstitial positions of the matrix tetragonal tungsten bronze phase during the solidification process. The second phase was distributed primarily at the edge site of the matrix grains, which modified the original columnar-shaped grains by inhibiting the growth of special crystal planes. With the help of fined-grains and core-shell structure induced by the second phase precipitation design, an energy density of 12.2 J/cm^3 with an efficiency of 89.5 % was achieved in the $SrBaTiNb_{1.9}Ta_{0.1}O_9$ ceramic [83]. Another dual-phase strategy proposed by Xiong et al. is to construct a dual-phase structure through *in situ* phase separation. Unlike the multiphase structure of phases with different electrical properties, the authors fabricated a grain-separated two-perovskite phase structure by a conventional solid-state reaction method. With strong interaction between these two RFE phases, the structural design featured diversified nanoscale polar structures and heterogeneous grain boundaries, which synergistically promoted high polarization with low hysteresis, greatly increased resistivity, and suppressed electrical strain. Therefore, a high energy density of 23.6 J/cm^3 with an efficiency of 92 % under 990 kV/cm was achieved in the 0.5BNT-0.4BT-$0.1CdZrO_3$ bulk ceramic capacitor (Fig. 6G, H, I, J) [84]. Core-shell structure with separate components can fabricated by introducing end members of ions with various radii or excess additives [85]. Wang et al. fabricated $0.62BiFeO_3$-$0.3BaTiO_3$-$0.08Nd(Zn_{0.5}Zr_{0.5})O_3$ ceramics with a core-shell grain structure. Due to the different diffusion rates and thermal expansion coefficients of different elements during sintering and cooling, various elements were selectively segregated in the core and shell regions. Although the core and shell regions were not the same chemically, a certain continuity in their composition led to the electrical uniformity of the ceramic under the condition of uneven chemical composition. The multilayered ceramics demonstrated an ultrahigh discharge energy density (W_{dis} = 10.5 J/cm^3) with a high efficiency of 87 % [86]. Similarly, Zhang et al. prepared a core-shell structure by introducing excessive MgO in grain boundaries. The formed second phase can effectively enhance the E_b, induce the antiferroelectric to ferroelectric transition, and stabilize the antiferroelectric phase under electric field loading [87].

In summary, multi-phase engineering can increase chemical and

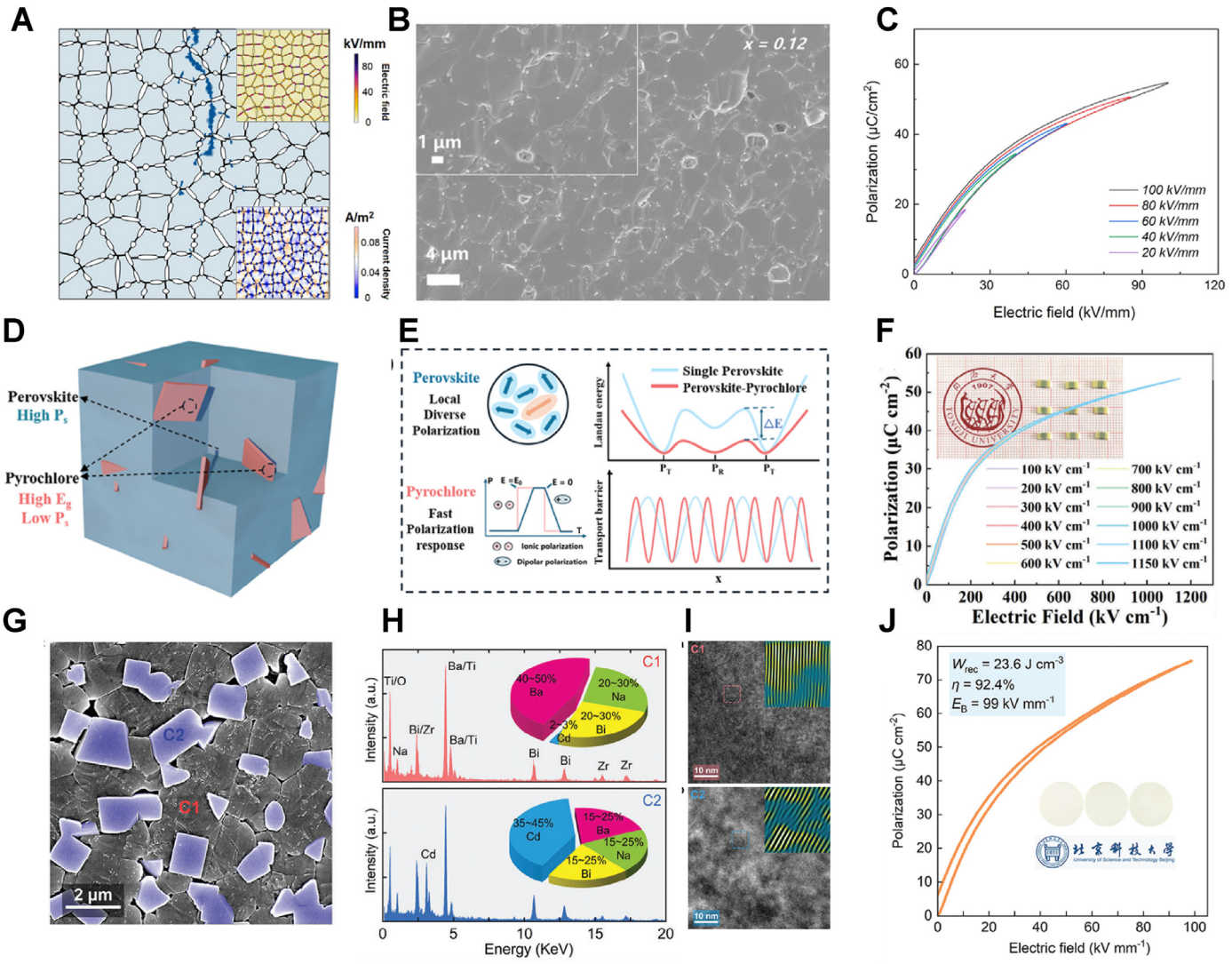

Fig. 6. Simulated electrical breakdown pathways. (A) The nanoisland-like microstructure. (B) SEM of the $0.52BaTiO_3$-$0.36BiFeO_3$-$0.12CaTiO_3$. (C) *P-E* loops of the multilayer ceramic capacitors. A, B, and C are reproduced from Ref. [82] with permission. (D) Structure of perovskite–pyrochlore multiphase ceramics. (E) Schematic diagram of the correlation between the microstructure, polarization, and breakdown field strength in perovskite-pyrochlore multiphase ceramics. (F) *P–E* loops recorded for the $(Bi_{0.5}Na_{0.5})_{0.65}(Sr_{0.7}Bi_{0.2})_{0.35}Ti_{0.88}Hf_{0.12}O_3$ MLCCs under different electric field. D, E, and F are reproduced from Ref. [27] with permission. (G) SEM micrograph. (H) EDS patterns. (I) HR-TEM images recorded along $[110]_c$ direction. (J) Unipolar *P–E* loop under breakdown field of dual-phase $0.5BNT$-$0.4BT$-$0.1CdZrO_3$ ferroelectric ceramic. G, H, I, and J are reproduced from Ref. [84] with permission.

electrical heterogeneity, and modify grain shape and size, thereby helping modify the ferroelectric behavior and enhance the E_b; however, introducing of unevenly distributed second phases may lead to the poor matching of phase interfaces and defect aggregation, reducing E_b as well as resistivity at high temperature.

7. Core-shell structure design

Despite numerous efforts that have been made to explore novel dielectric ceramics with better energy storage performance, materials with high polarization with high breakdown strength seem to be out of reach due to the essential negative correlation between ε_r and E_b. In this case, heterogeneous dielectric designs that combine the characteristics of serval dielectric are considered by an increasing number of researchers. Among them, the core-shell structure design is a common and reliable method to combine the characteristics of different dielectric materials and has attracted growing attention to improving the energy storage performance of dielectric materials.

In inorganic ferroelectric ceramic composites with core-shell structure, the simple oxide is broadly utilized to coat on dielectrics by chemical coating method as the "shell" [88,89]. For instance, Wang et al. reported $BaTiO_3$@NiO dielectric ceramics, where $BaTiO_3$ was the "core" nanoparticles and NiO was the "shell" surrounding [90]. Such 1 % NiO-added ceramics with core-shell structure exhibited an antiferroelectric-like feature, although barium titanate is a traditional ferroelectric material. High-densification microstructures with fine-crystalline and uniform distribution are obtained and reach an energy density of 2.72 J/cm^3 with low remnant polarization. Zhu et al. reported $0.78Bi_{0.5}Na_{0.5}TiO_3$-$0.22NaNbO_3$(BNT-NN) @0.8 wt%$SiO_2$ ceramics with a large discharge energy density of 6.17J/cm^3 at a relatively low electric field of 330 kV/cm and displayed high temperature stability of permittivity from 35 to 400 °C [91]. Compared to samples without the SiO_2 shell layer, E_b exhibits a remarkable 50 % increase that results from the finer grain size and enhanced band gap, while still maintaining high polarization. Huan et al. reported $0.95K_{0.5}Na_{0.5}NbO_3$–$0.05Bi(Zn_{0.5}Ti_{0.5})O_3$ @3.5 wt% SiO_2 dielectric ceramics with significant improvement of the breakdown strength and fatigue durability [92]. The simulation-supported experimental results declared that this core-shell

structure increases the bending strength and compression strength of samples by more than 50 % compared to samples without "shell" structure, with a large reduction of electric field-induced strain that suppresses electrical deformation, as shown in Fig. 7A. As a result, generation and propagation of cracks was restrained, and thus samples reached E_b of 425 kV/cm and recoverable energy density of 4.64 J/cm^3, with variation of recoverable energy density< ±2 % after 10^5 cycles. Wu et al. developed a phase-field model, with antiferroelectric as the core and linear dielectric as the shell, as shown in Fig. 7B [93]. Compared to pure samples, the sample with a core-shell structure had a slanted hysteresis loop of polarization with delayed saturation polarization, decreased maximum polarization, and hysteresis loss. With increasing shell fraction and lower low shell permittivity, this phenomenon became more distinct and led to the vanishment of the hysteresis loop. It was also determined that various shell parameters can contribute to the difference in the antiferroelectric polarization and thus affect the energy storage characteristics. As a result, certain core-shell samples have much higher energy density and efficiency than pure samples.

Furthermore, special designs on shell structures and compositions can be considered. Yuan et al. reported BT-Bi($Mg_{0.5}Zr_{0.5}$)O_3@SiO_2 dielectric ceramic with a raspberry-like hierarchical structure [94]. Such a bio-inspired structure design enables samples to have synergistically improved large E_b with sustained large polarization, and the result was proved by both experimental characterizations and theoretical simulations. Zhang et al. reported $Na_{0.4}K_{0.1}Bi_{0.5}$-TiO_3@$SrZrO_3$(SZ)-$BiMg_{0.5}Sn_{0.5}O_3$(BMS)@SiO_2 dielectric ceramic with double "shell", as shown in Fig. 7C, where SZ-BMS phase could alleviate interfacial polarization, reconstruct domain and adjust defect, and SiO_2 shell in outer is helpful for grain size refinement and defect control [95]. The synergy effect between each shell and core led to a high recoverable energy density of 3.94 J/cm^3 with a high efficiency of 87.1 %.

The core-shell structure can also be induced and formed through chemical heterogeneity to improve the temperature stability of ceramic capacitors [28] and is a feasible way to improve energy storage performance as well. Huang reported 0.93$Ba_{0.55}Sr_{0.39}Zn_{0.06}TiO_3$-0.07-$BiMg_{2/3}Nb_{1/3}O_3$ that exhibited a recoverable energy density of 5.92 J/cm^3 with efficiency of 81.7 % [96]. Using two-step calcination, heterogeneous microstructures are induced, resulting from destruction of the cooperative diffusion effect of multiple ions. Doping of Zn^{2+} enhanced the probability for off-centering of ions, leading to a higher contribution of dielectric displacement and relaxor ferroelectric domain switching to Pmax. Compared to samples without core-shell structure, structural difference was the main reason for the improvement in E_b, since electric trees preferred propagating along the shell and the effective path for propagation was thus prolonged. Such results were proven by both experiment and simulation. Dong et al. reported 0.6[0.90NaNbO$_3$-0.10Bi($Mg_{2/3}Nb_{1/3}$)O_3]-0.4($Bi_{0.5}Na_{0.5}$)$_{0.7}Sr_{0.3}TiO_3$ dielectric ceramics with recoverable energy density of 7.72 J/cm^3 and efficiency of 83.78 % [97]. Phase-field simulations indicated that the presence of a polar core effectively reduced the local electric field distribution of the shell with poor polar, leading to the improvement of E_b. First-principles calculations based on density functional theory further analyzed the improvement of E_b. Moreover, strong polar and weak polar clusters that presented in grains with composition inhomogeneity enhanced the

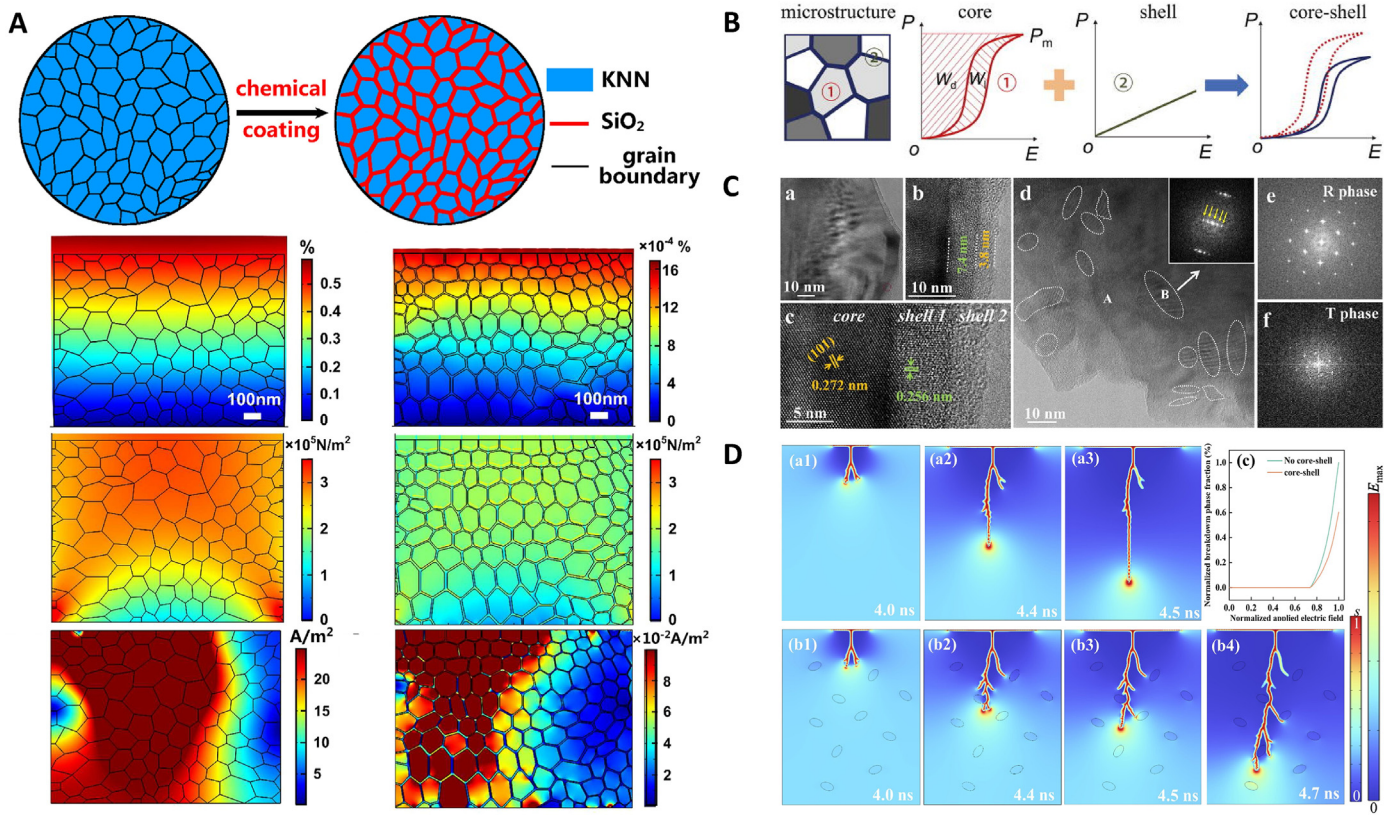

Fig. 7. (A) Schematic diagrams for KNN ceramic in left column and KNN@SiO_2 ceramic in right column. Diagrams in the first row represent the grain configuration. Diagrams in the second row represent the electrostrictive strain under the same electric field. Diagrams in the third row represent the stress distribution under the same loading conditions, and diagrams in the fourth row represent the simulated breakdown path. Reproduced from Ref. [92] with permission. (B) Schematic for the simulated core-shell antiferroelectric ceramics, with illustration of microstructure, and the *P-E* loop of each part and the combination. Reproduced from Ref. [93] with permission. (C) Bright-field TEM image of ceramic samples with 15 mol% BMS coating, indicating the presence of double shell structure, showing the distribution of nanodomains. Reproduced from Ref. [95] with permission. (D) Simulation of local electric field distribution and breakdown pathways at various moments for (a1-a3) ceramic without core-shell structure and (b1–b4) ceramic with core-shell structure, (c) showing the nominal applied electric field vs. nominal breakdown phase area fraction of ceramics with different structures. Reproduced from Ref. [98] with permission.

polarization difference, and all underlying mechanisms contributed to the improved energy storage performance. Li et al. reported 0.2$BiFeO_3$-0.8($Ba_{0.2}S_{r0.2}Ca_{0.2}Bi_{0.2}Na_{0.2}$)$TiO_3$ MLCC with a high recoverable energy density of 12.1 J/cm^3 with the efficiency of 86.1 % [98]. Such high energy storage performance results from the synergy effect of refined grain size, broadened band gap, and core-shell microstructure. To further understand the mechanisms of core-shell structures that affect the breakdown behavior of dielectric, a phase-field breakdown model was developed to simulate the distribution and evolution of the electric tree in ceramics with or without core-shell structures, as shown in Fig. 7D. The results indicated that core-shell structures can effectively reduce the breakdown phase, since high applied electric field mainly concentrates on "core" with high permittivity and weakens the local electric field of the shell.

In general, the core-shell structure design is available to apply during the optimization of energy storage dielectric, which can tune the ferroelectric behavior, restrict the growth of grain, and increase the E_b. Nevertheless, the presence of interface effects between the core and shell, as well as relevant mechanisms needs to be further studied.

8. Multilayer structural design

Multilayer ceramic structures have emerged as a critical approach to optimize dielectric and energy storage properties in advanced capacitors and energy storage systems. Multilayer architectures, achieved through tape casting and lamination, provide flexibility in tailoring material properties. These structures enable enhancements in dielectric constants, breakdown strength, and energy storage density while ensuring thermal and frequency stability. Layered ceramics maximize energy storage performance through optimized polarization and electric field distribution. Interfaces in multilayer ceramics redistribute the electric field, reducing local stresses and enhancing breakdown strength. Yuan et al. demonstrated that the structure of $BaTiO_3$/$BaTiO_3$@SiO_2 layered ceramic enhanced the dielectric constant and boosted breakdown strength through electric field redistribution and the interface blocking effect, as shown in Fig. 8A [29]. Yang et al. developed a sandwiched structure featuring a negative dielectric layer made from materials exhibiting negative permittivity, which significantly enhanced interfacial polarization and increased overall permittivity, as shown in Fig. 8B [99]. The

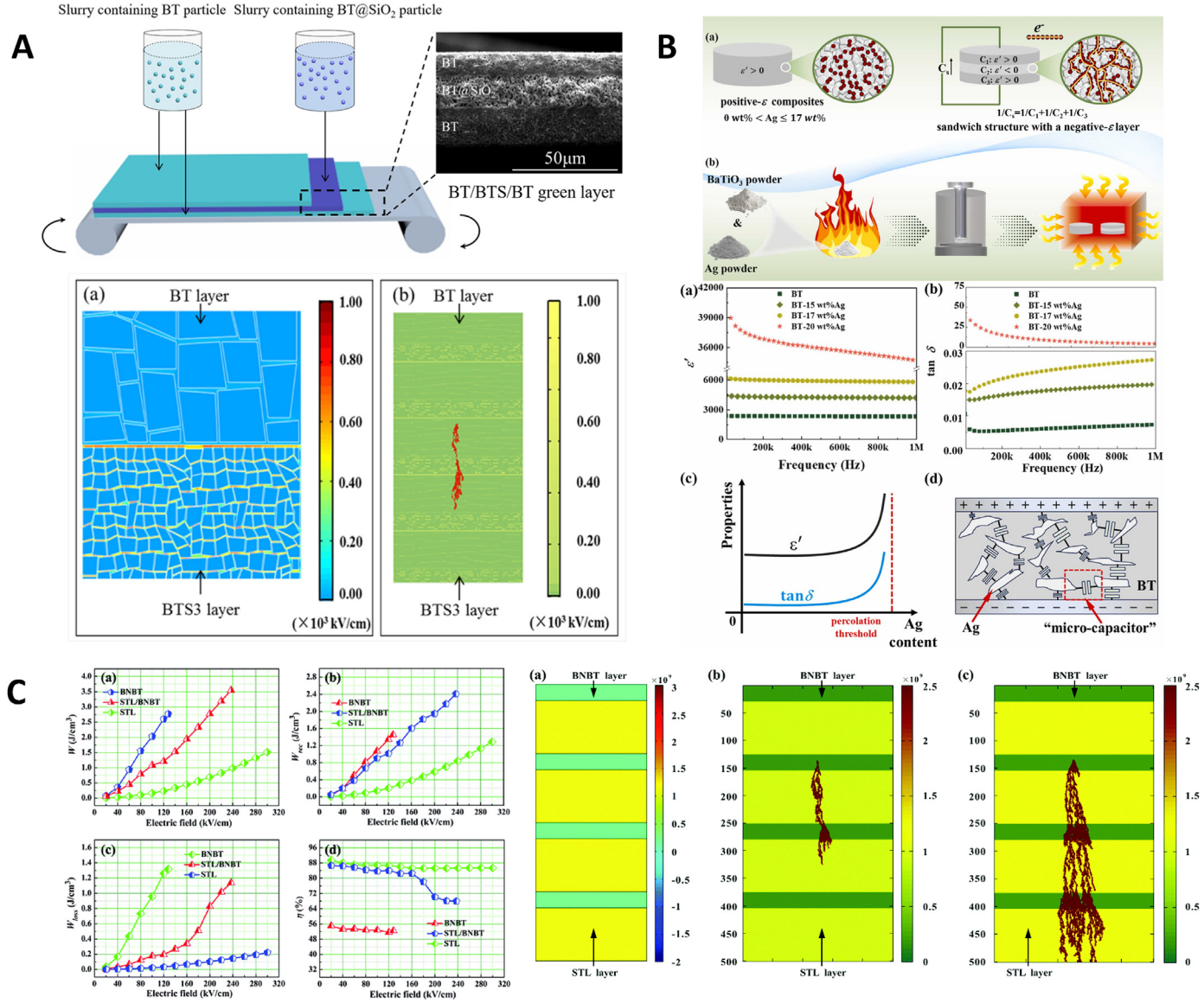

Fig. 8. (A) Schematic diagram for fabricating BT/BT@SiO_2/BT layers and finite element simulated results for BT/BT@SiO_2 layered ceramics. Reproduced from Ref. [29] with permission. (B) Synthesis schematic diagram, dielectric properties, and a schematic diagram showing the role of Ag. Reproduced from Ref. [99] with permission. (C) The model of electrical tree propagation and dielectric properties. Reproduced from Ref. [100] with permission.

sandwich design effectively suppressed dielectric loss by inhibiting the formation of conductive pathways along the electric field direction. The permittivity of $BaTiO_3$/Ag ceramics reached 8000 with the dielectric loss below 0.02. Yan et al. found that the dielectric constant of the layered $(SrTiO_3+Li_2CO_3)/(0.94Bi_{0.54}Na_{0.46}TiO_3\text{-}0.06BaTiO_3)$ (STL/BNBT) ceramic surpasses that of pure STL or BNBT, exhibiting excellent frequency stability [100]. This multilayer structure significantly improved both breakdown strength and maximum polarization, as shown in Fig. 8C. The STL/BNBT multilayer ceramic achieved a maximum W_{rec} of 2.41 J/cm^3 at 237 kV/cm, with relaxor behavior. Yan et al. reported a sandwich structure comprising ferroelectrics with large polarization as the outer layer and the linear-like dielectric with large E_b as the middle layer to optimize both the polarization and E_b in dielectrics and achieve a high energy density of 6.78 J/cm^3 with an efficiency of 89.7 % [101].

Multilayer designs also result in homogenized dielectric properties. Jin et al. discovered that compositionally graded ceramics $(1\text{-}x)(Bi_{0.85}La_{0.15})FeO_3\text{–}xPbTiO_3$ exhibited uniform dielectric properties by gradually varying material composition across layers [102]. This results in reduced dielectric loss and enhanced strain response. Chao et al. developed $BaTiO_3/SrTiO_3$ multilayers with a compositional gradient through tape-casting and lamination, optimizing dielectric properties such as maximum dielectric constant, loss tangent, TCC, and *P–E* relationships by adjusting the spatial arrangement of $BaTiO_3$ and $SrTiO_3$ layers [103]. Miao et al. reported significant deviations in the dielectric properties of $(Ba_{0.95}Ca_{0.05})(Zr_{0.15}Ti_{0.842}Mg_{0.008})O_3$- $(Ba_{0.95}Ca_{0.05})(Zr_{0.08}Ti_{0.92})O_3$ layered ceramics from theoretical predictions, attributed to idealized assumptions in the simulations and grain size variations compared to the pure single phase [104].

Multilayer ceramic architecture represents a versatile approach to advancing dielectric and energy storage technologies. By leveraging compositional grading, interface engineering, and precision fabrication, these materials achieve enhanced performance metrics critical for high-reliability applications.

9. Conclusion

We have summarized the typical designs of microstructure that are applied in the optimizations of energy storage dielectrics ceramic and show the strong correlation between microstructure and energy storage performance. Despite numerous microstructural studies that have advanced the development of energy storage dielectric ceramics, an understanding of relationships between the microstructures and properties of dielectrics is still insufficient. Future research on microstructure designs can be deeply conducted in the following aspects:

(1) *Combination of different microstructure design in multiscale*

Numerous research has been carried out on microstructure designs to improve the performance of energy storage dielectrics. Nevertheless, microstructure designs in multiscale are rarely mentioned. Recently, multiscale optimization strategies [105] with designs in scales such as atomic scale, grain scale, device scale have been utilized to improve energy storage performance. It is illustrated that a combination of different microstructure designs in multiscale can be a universal approach to improve the energy storage performance in dielectric, especially in devices of MLCC. However, it is still difficult to clarify the role of different microstructures and to achieve an optimal combination. More theoretical research and experimental exploration are needed to achieve a hierarchical design in multiscale microstructures.

(2) *Improvement of modeling*

In recent decades, through the rapid development of computing technology and the related theory of dielectric, there have been complex simulation and modeling including density functional theory, phase-field simulation, or finite element simulation become available in research of dielectrics, which have been widely used by researchers to study, e.g., breakdown behavior and relaxation behavior of dielectrics. The relevant results of simulations can be used to guide rational microstructure designs of dielectrics. However, multiscale modeling and simulation are still difficult to achieve, for example, how to model composition-induced microstructures of multiscale and to study a variety of properties and behaviors including breakdown and polarization. The improvement of relevant theories and simulation methods remains of challenge and more research is needed.

(3) *Establishment of database for machine learning*

Machine learning is regarded as an efficient method for discovering novel material systems. With a combination of high-throughput computing techniques, the composition and properties of candidate materials can be quickly screened and analyzed. Such comprehensive technology can also extend to microstructure designs, which has considerable potential to obtain mathematical expressions for semi or fully quantitatively predicting different properties of specific microstructures and can thus omit tedious experimental exploration, saving cost and improving efficiency. To achieve this, establishing new databases that include information of different microstructures with their relevant properties is necessary. Increasingly mature intelligent algorithms can also be introduced to speed up the establishment of databases, enhance the efficiency of machine learning, and further guide the development of experiments.

CRediT authorship contribution statement

Minhao Zhang: Writing – original draft. **Jinquan Zeng:** Writing – original draft. **Yiying Chen:** Writing – original draft. **Shun Lan:** Writing – review & editing. **Yan Song:** Writing – review & editing. **Yuanhua Lin:** Writing – review & editing, Project administration.

Declaration of competing interest

The authors declare that they have no known competing financial interests or personal relationships that could have appeared to influence the work reported in this paper.

Acknowledgements

This work was supported by the National Key Research Program of China (Grant No. 2021YFB3800601), the Basic Science Center Project of the National Natural Science Foundation of China (Grant No. 52388201), and the Shuimu Tsinghua Scholar Program of Tsinghua University.

References

[1] Q.K. Feng, S.L. Zhong, J.Y. Pei, Y. Zhao, D.L. Zhang, D.F. Liu, Y.X. Zhang, Z.M. Dang, Recent progress and future prospects on all-organic polymer dielectrics for energy storage capacitors, Chem. Rev. 122 (2021) 3820–3878, https://doi.org/10.1021/acs.chemrev.1c00793.

[2] M.J. Feng, Y. Feng, T.D. Zhang, J.L. Li, Q.G. Chen, Q.G. Chi, Q.Q. Lei, Recent advances in multilayer-structure dielectrics for energy storage application, Adv. Sci. 8 (2021) 2102221, https://doi.org/10.1002/advs.202102221.

[3] F. Yan, J. Qian, S.M. Wang, J.W. Zhai, Progress and outlook on lead-free ceramics for energy storage applications, Nano, Energy 123 (2024) 109394, https://doi.org/10.1016/j.nanoen.2024.109394.

[4] L.T. Yang, X. Kong, F. Li, H. Hao, Z.X. Cheng, H.X. Liu, J.F. Li, S.J. Zhang, Perovskite lead-free dielectrics for energy storage applications, Prog. Mater. Sci. 102 (2019) 72–108, https://doi.org/10.1016/j.pmatsci.2018.12.005.

[5] G. Wang, Z.L. Lu, Y. Li, L.H. Li, H.F. Ji, A. Feteira, D. Zhou, D.W. Wang, S.J. Zhang, I.M. Reaney, Electroceramics for high-energy density capacitors: current status and future perspectives, Chem. Rev. 121 (2021) 6124–6172, https://doi.org/10.1021/acs.chemrev.0c01264.

[6] L. Chen, S.Q. Deng, H. Liu, J. Wu, H. Qi, J. Chen, Giant energy-storage density with ultrahigh efficiency in lead-free relaxors via high-entropy design, Nat. Commun. 13 (2022) 3089, https://doi.org/10.1038/s41467-022-30821-7.

[7] Z.L. Lu, W.C. Bao, G. Wang, S.K. Sun, L.H. Li, J.L. Li, H.J. Yang, H.F. Ji, A. Feteira, D.J. Li, F.F. Xu, A.K. Kleppe, D.W. Wang, S.Y. Liu, I.M. Reaney, Mechanism of

enhanced energy storage density in $AgNbO_3$-based lead-free antiferroelectrics, Nano, Energy 79 (2021) 105423, https://doi.org/10.1016/j.nanoen.2020.105423.
[8] A.W. Xie, J. Fu, R.Z. Zuo, X.W. Jiang, T.Y. Li, Z.Q. Fu, Y.W. Yin, X.G. Li, S.J. Zhang, Supercritical relaxor nanograined ferroelectrics for ultrahigh-energy-storage capacitors, Adv. Mater. 34 (2022) 2204356, https://doi.org/10.1002/adma.202204356.
[9] M. Zhang, H.B. Yang, Y. Lin, Q.B. Yuan, H.L. Du, Significant increase in comprehensive energy storage performance of potassium sodium niobate-based ceramics via synergistic optimization strategy, Energy Storage Mater. 45 (2022) 861–868, https://doi.org/10.1016/j.ensm.2021.12.037.
[10] J. Guo, H.F. Yu, Y.F. Ren, H. Qi, X.R. Yang, Y. Deng, S.T. Zhang, J. Chen, Multi-symmetry high-entropy relaxor ferroelectric with giant capacitive energy storage, Nano, Energy 112 (2023) 108458, https://doi.org/10.1016/j.nanoen.2023.108458.
[11] J. Chen, Y. Zhou, X.Y. Huang, C.Y. Yu, D.L. Han, A. Wang, Y.K. Zhu, K.M. Shi, Q. Kang, P.L. Li, P.K. Jiang, X.S. Qian, H. Bao, S.T. Li, G.N. Wu, X.Y. Zhu, Q. Wang, Ladderphane copolymers for high-temperature capacitive energy storage, Nature 615 (2023) 62–66, https://doi.org/10.1038/s41586-022-05671-4.
[12] R. Wang, Y.J. Zhu, J. Fu, M.C. Yang, Z.Y. Ran, J.L. Li, M.X. Li, J. Hu, J.L. He, Q. Li, Designing tailored combinations of structural units in polymer dielectrics for high-temperature capacitive energy storage, Nat. Commun. 14 (2023) 2406, https://doi.org/10.1038/s41467-023-38145-w.
[13] C. Wu, A.A. Deshmukh, Z.Z. Li, L.H. Chen, A. Alamri, Y.F. Wang, R. Ramprasad, G.A. Sotzing, Y. Cao, Flexible temperature-invariant polymer dielectrics with large bandgap, Adv. Mater. 32 (2020) 2000499, https://doi.org/10.1002/adma.202000499.
[14] H. Li, H.B. Zheng, T.L. Yue, Z.L. Xie, S.P. Yu, J. Zhou, T. Kapri, Y.F. Wang, Z.Q. Cao, H.Y. Zhao, A. Kemelbay, J.L. He, G. Zhang, P.F. Pieters, E.A. Dailing, J.R. Cappiello, M. Salmeron, X.D. Gu, T. Xu, P. Wu, Y. Li, K.B. Sharpless, Y. Liu, Machine learning-accelerated discovery of heat-resistant polysulfates for electrostatic energy storage, Nat. Energy 10 (2025) 90–100, https://doi.org/10.1038/s41560-024-01670-z.
[15] S. Shukla, C. Wu, A. Mishra, J.K. Pan, A.P. Charnay, A. Khomane, A. Deshmukh, J.R. Zhou, M. Mukherjee, R. Gurnani, P. Rout, R. Casalini, R. Ramprasad, M.D. Fayer, P. Vashishta, Y. Cao, G. Sotzing, Pendant group functionalization of cyclic olefin for high temperature and high-density energy storage, Adv. Mater. 36 (2024) 2402133, https://doi.org/10.1002/adma.202402133.
[16] J.F. Dong, R.C. Hu, X.W. Xu, J. Chen, Y.J. Niu, F. Wang, J.Y. Hao, K. Wu, Q. Wang, H. Wang, A facile in situ surface-functionalization approach to scalable laminated high-temperature polymer dielectrics with ultrahigh capacitive performance, Adv. Funct. Mater. 31 (2021) 2102644, https://doi.org/10.1002/adfm.202102644.
[17] B. Zhang, X.M. Chen, Z. Pan, P. Liu, M.M. Mao, K.X. Song, Z. Mao, R. Sun, D.W. Wang, S.J. Zhang, Superior high-temperature energy density in molecular semiconductor/polymer all-organic composites, Adv. Funct. Mater. 33 (2023) 2210050, https://doi.org/10.1002/adfm.202210050.
[18] Y.J. Niu, J.F. Dong, Y.F. He, X.W. Xu, S. Li, K. Wu, Q. Wang, H. Wang, Significantly enhancing the discharge efficiency of sandwich-structured polymer dielectrics at elevated temperature by building carrier blocking interface, Nano Energy 97 (2022) 107215, https://doi.org/10.1016/j.nanoen.2022.107215.
[19] W.Y. Zhou, G.Z. Cao, M.X. Yuan, S.L. Zhong, Y.D. Wang, X.R. Liu, D. Cao, W.W. Peng, J. Liu, G.H. Wang, Z.M. Dang, B. Li, Core-shell engineering of conductive fillers toward enhanced dielectric properties: a universal polarization mechanism in polymer conductor composites, Adv. Mater. 35 (2023) 2207829, https://doi.org/10.1002/adma.202207829.
[20] L.L. Ren, H. Li, Z.L. Xie, D. Ai, Y. Zhou, Y. Liu, S.Y. Zhang, L.J. Yang, X.T. Zhao, Z.R. Peng, R.J. Liao, Q. Wang, High-temperature high-energy-density dielectric polymer nanocomposites utilizing inorganic core-shell nanostructured nanofillers, Adv. Energy Mater. 11 (2021) 2101297, https://doi.org/10.1002/aenm.202101297.
[21] Z.J. Yang, D. Yue, Y.H. Yao, J.L. Li, Q.G. Chi, Q.G. Chen, D.M. Min, Y. Feng, Energy storage application of all-organic polymer dielectrics: a review, Polymers 14 (2022) 1160, https://doi.org/10.3390/polym14061160.
[22] D.W. Wang, D. Zhou, K.X. Song, A. Feteira, C.A. Randall, I.M. Reaney, Cold-sintered C0G multilayer ceramic capacitors, Adv. Electron. Mater. 5 (2019) 1900025, https://doi.org/10.1002/aelm.201900025.
[23] M.J. Pan, C.A. Randall, A brief introduction to ceramic capacitors, IEEE Electr. Insul. Mag. 26 (2010) 44–50, https://doi.org/10.1109/MEI.2010.5482787.
[24] M. Zhang, S. Lan, B.B. Yang, H. Pan, Y.Q. Liu, Q.H. Zhang, J.L. Qi, D. Chen, H. Su, D. Yi, Y.Y. Yang, R. Wei, H.D. Cai, H.J. Han, L. Gu, C.W. Nan, Y.H. Lin, Ultrahigh energy storage in high-entropy ceramic capacitors with polymorphic relaxor phase, Science 384 (2024) 185–189, https://doi.org/10.1126/science.adl2931.
[25] Y.Y. Chen, J.L. Qi, M.H. Zhang, Z.X. Luo, Y.H. Lin, Pyrochlore-based high-entropy ceramics for capacitive energy storage, J. Adv. Ceram. 11 (2022) 1179–1185, https://doi.org/10.1007/s40145-022-0613-3.
[26] J.L. Li, Z.H. Shen, X.H. Chen, S. Yang, W.L. Zhou, M.W. Wang, L.H. Wang, Q.W. Kou, Y.C. Liu, Q. Li, Z. Xu, Y.F. Chang, S.J. Zhang, F. Li, Grain-orientation-engineered multilayer ceramic capacitors for energy storage applications, Nat. Mater. 19 (2020) 999–1005, https://doi.org/10.1038/s41563-020-0704-x.
[27] S.M. Wang, J. Qian, G.L. Ge, F.Q. Zhang, F. Yan, J.F. Lin, L.M. Tang, M.H. Yang, Z.B. Pan, X. Wei, B. Shen, Z.F. Liu, J.W. Zhai, Embedding Plate-like pyrochlore in perovskite phase to enhance energy storage performance of BNT-based ceramic capacitors, Adv. Energy Mater. 15 (2025) 2403926, https://doi.org/10.1002/aenm.202403926.
[28] S.C. Jeon, B.K. Yoon, K.H. Kim, S.J.L. Kang, Effects of core/shell volumetric ratio on the dielectric-temperature behavior of $BaTiO_3$, J. Adv. Ceram. 3 (2014) 76–82, https://doi.org/10.1007/s40145-014-0096-y.
[29] Q.B. Yuan, J. Cui, Y.F. Wang, R. Ma, H. Wang, Significant enhancement in breakdown strength and energy density of the $BaTiO_3$/$BaTiO_3$@SiO_2 layered ceramics with strong interface blocking effect, J. Eur. Ceram. Soc. 37 (2017) 4645–4652, https://doi.org/10.1016/j.jeurceramsoc.2017.06.028.
[30] B.B. Yang, Q.H. Zhang, H.B. Huang, H. Pan, W.X. Zhu, F.Q. Meng, S. Lan, Y.Q. Liu, B. Wei, Y.Q. Liu, L.T. Yang, L. Gu, L.Q. Chen, C.W. Nan, Y.H. Lin, Engineering relaxors by entropy for high energy storage performance, Nat. Energy 8 (2023) 956–964, https://doi.org/10.1038/s41560-023-01300-0.
[31] H. Pan, F. Li, Y. Liu, Q.H. Zhang, M. Wang, S. Lan, Y.P. Zheng, J. Ma, L. Gu, Y. Shen, P. Yu, S.J. Zhang, L.Q. Chen, Y.H. Lin, C.W. Nan, Ultrahigh-energy density lead-free dielectric films via polymorphic nanodomain design, Science 365 (2019) 578–582, https://doi.org/10.1126/science.aaw8109.
[32] H. Qi, R.Z. Zuo, Linear-like lead-free relaxor antiferroelectric $(Bi_{0.5}Na_{0.5})TiO_3$-$NaNbO_3$ with giant energy-storage density/efficiency and super stability against temperature and frequency, J. Mater. Chem. A 7 (2019) 3971–3978, https://doi.org/10.1039/C8TA12232F.
[33] J. Jiang, X.J. Meng, L. Li, J. Zhang, S. Guo, J. Wang, X.H. Hao, H.G. Zhu, S.T. Zhang, Enhanced energy storage properties of lead-free $NaNbO_3$-based ceramics via A/B-site substitution, Chem. Eng. J. 422 (2021) 130130, https://doi.org/10.1016/j.cej.2021.130130.
[34] F.Z. Yao, Q.B. Yuan, Q. Wang, H. Wang, Multiscale structural engineering of dielectric ceramics for energy storage applications: from bulk to thin films, Nanoscale 12 (33) (2020) 17165–17184, https://doi.org/10.1039/D0NR04479B.
[35] A.A. Bokov, Z.G. Ye, Recent progress in relaxor ferroelectrics with perovskite structure, J. Mater. Sci. 41 (2006) 31–52, https://doi.org/10.1007/s10853-005-5915-7.
[36] B. Deka, K.H. Cho, $BiFeO_3$-Based relaxor ferroelectrics for energy storage: progress and prospects, Materials 14 (2021) 7188, https://doi.org/10.3390/ma14237188.
[37] S. Pattipaka, Y. Lim, Y.H. Son, Y.M. Bae, M. Peddigari, G.T. Hwang, Ceramic-based dielectric materials for energy storage capacitor applications, Materials 17 (2024) 2277, https://doi.org/10.3390/ma17102277.
[38] C. Liang, C.Y. Wang, H.Y. Zhao, W.J. Cao, X.C. Huang, C.C. Wang, Enhanced energy storage performance of $NaNbO_3$-based ceramics via band and domain engineering, Ceram. Int. 49 (2023) 40326–40335, https://doi.org/10.1016/j.ceramint.2023.10.005.
[39] H.C. Thong, Z. Li, J.T. Lu, C.B.W. Li, Y.X. Liu, Q.N. Sun, Z.Q. Fu, Y. Wei, K. Wang, Domain engineering in bulk ferroelectric ceramics via mesoscopic chemical inhomogeneity, Adv. Sci. 9 (2022) 2200998, https://doi.org/10.1002/advs.202200998.
[40] Z.Q. Lv, T. Lu, Z. Liu, T.F. Hu, Z.C. Hong, S.B. Guo, Z.Q. Xu, Y.X. Song, Y.H. Chen, X.Y. Zhao, Z.S. Lin, D.H. Yu, Y. Liu, G.S. Wang, $NaNbO_3$-Based multilayer ceramic capacitors with ultrahigh energy storage performance, Adv. Energy Mater. 14 (2024) 2304291, https://doi.org/10.1002/aenm.202304291.
[41] Q.Y. Zheng, B. Xie, Y.H. Tian, Q. Wang, H.J. Luo, Z.Y. Liu, H.B. Zhang, High recoverable energy density of $Na_{0.5}Bi_{0.5}TiO_3$-based ceramics by multi-scale insulation regulation and relaxor optimization strategy, J. Materiomics. 10 (2024) 845–856, https://doi.org/10.1016/j.jmat.2023.10.005.
[42] J. Jiang, X.J. Meng, L. Li, S. Guo, M. Huang, J. Zhang, J. Wang, X.H. Hao, H.G. Zhu, S.T. Zhang, Ultrahigh energy storage density in lead-free relaxor antiferroelectric ceramics via domain engineering, Energy Storage Mater. 43 (2021) 383–390, https://doi.org/10.1016/j.ensm.2021.09.018.
[43] Y. Zhang, G.R. Zhang, A. Li, Z.N. Wang, Y.Q. Zheng, G.Q. Luo, R. Tu, J. Zhang, Q. Shen, L.M. Zhang, Improved energy storage performance of lead-free $BaTi_{0.96}Li_{0.04}O_{2.94}$ ceramics via domain structure engineering, Ceram. Int. 49 (2023) 28201–28207, https://doi.org/10.1016/j.ceramint.2023.06.073.
[44] Z.M. Cai, X.H. Wang, W. Hong, B.C. Luo, Q.C. Zhao, L.T. Li, Grain-size-dependent dielectric properties in nanograin ferroelectrics, J. Am. Ceram. Soc. 101 (2018) 5487–5496, https://doi.org/10.1111/jace.15803.
[45] T. Tunkasiri, G. Rujijanagul, Dielectric strength of fine grained barium titanate ceramics, J. Mater. Sci. Lett. 15 (1996) 1767–1769, https://doi.org/10.1007/BF00275336.
[46] H.Y. Lee, K.H. Cho, H.D. Nam, Grain size and temperature dependence of electrical breakdown in $BaTiO_3$ ceramic, Ferroelectrics 334 (2006) 165–169, https://doi.org/10.1080/00150190600694415.
[47] R. Waser, The role of grain-boundaries in conduction and breakdown of perovskite-type titanates, Ferroelectrics 133 (1992) 109–114, https://doi.org/10.1080/00150199208217984.
[48] C.Y. Wang, W.J. Cao, C. Liang, H.Y. Zhao, C.C. Wang, Equimolar high-entropy for excellent energy storage performance in $Bi_{0.5}Na_{0.5}TiO_3$-based ceramics, Energy Storage Mater. 70 (2024) 103534, https://doi.org/10.1016/j.ensm.2024.103534.
[49] Z. Sun, H. Liu, J. Zhang, H.J. Luo, Y.H. Yao, Y.P. Zhang, L.J. Liu, J.C. Neuefeind, J. Chen, Strong local polarization fluctuations enabled high electrostatic energy storage in Pb-free relaxors, J. Am. Chem. Soc. 146 (2024) 13467–13476, https://doi.org/10.1021/jacs.4c02868.
[50] P.R. Ren, H. Zhao, X. Wang, Y.H. Wan, Z.Y. Liu, C.B. Long, F.X. Yan, T. Frömling, G.Y. Zhao, Super-stable permittivity and low dielectric loss of (1-x) $Na_{0.5}Bi_{0.5+y}TiO_3$-x$NaTaO_3$ ceramics within an ultra-wide temperature range, J. Materiomics. 9 (2023) 482–491, https://doi.org/10.1016/j.jmat.2022.12.004.
[51] S. Chattopadhyay, P. Ayyub, V.R. Palkar, M. Multani, Size-induced diffuse phase-transition in the nanocrystalline ferroelectric $PbTiO_3$, Phys. Rev. B 52 (1995) 13177–13183, https://doi.org/10.1103/PhysRevB.52.13177.
[52] C.Q. Zhu, X.H. Wang, Q.C. Zhao, Z.M. Cai, Z.Y. Cen, L.T. Li, Effects of grain size and temperature on the energy storage and dielectric tunability of non-reducible

$BaTiO_3$-based ceramics, J. Eur. Ceram. Soc. 39 (2019) 1142–1148, https://doi.org/10.1016/j.jeurceramsoc.2018.11.034.
[53] H. Ghayour, M. Abdellahi, A brief review of the effect of grain size variation on the electrical properties of $BaTiO_3$-based ceramics, Powder, Tech 292 (2016) 84–93, https://doi.org/10.1016/j.powtec.2016.01.030.
[54] W.W. Cao, C.A. Randall, Grain size and domain size relations in bulk ceramic ferroelectric materials, J. Phys. Chem. Solid. 57 (1996) 1499–1505, https://doi.org/10.1016/0022-3697(96)00019-4.
[55] L. Chen, T.F. Hu, X.M. Shi, H.F. Yu, H. Zhang, J. Wu, Z.Q. Fu, H. Qi, J. Chen, Near-zero energy consumption capacitors by controlling inhomogeneous polarization configuration, Adv. Mater. 36 (2024) 2313285, https://doi.org/10.1002/adma.202313285.
[56] N.N. Luo, L. Ma, G.G. Luo, C. Xu, L.X. Rao, Z.G. Chen, Z.Y. Cen, Q. Feng, X.Y. Chen, F. Toyohisa, Y. Zhu, J.W. Hong, J.F. Li, S.J. Zhang, Well-defined double hysteresis loop in $NaNbO_3$ antiferroelectrics, Nat. Commun. 14 (2023) 1776, https://doi.org/10.1038/s41467-023-37469-x.
[57] Q. Xu, D. Zhan, D.P. Huang, H.X. Liu, W. Chen, F. Zhang, Effect of MgO-CaO-Al_2O_3-SiO_2 glass additive on dielectric properties of $Ba_{0.95}Sr_{0.05}Zr_{0.2}Ti_{0.8}O_3$ ceramics, J. Alloys Compd. 558 (2013) 77–83, https://doi.org/10.1016/j.jallcom.2012.12.164.
[58] Q. Xu, J. Xie, Z.C. He, L. Zhang, M.H. Cao, X.D. Huang, M.T. Lanagan, H. Hao, Z.H. Yao, H.X. Liu, Energy-storage properties of $Bi_{0.5}Na_{0.5}TiO_3$-$BaTiO_3$-$KNbO_3$ ceramics fabricated by wet-chemical method, J. Eur. Ceram. Soc. 37 (2017) 99–106, https://doi.org/10.1016/j.jeurceramsoc.2016.07.011.
[59] X.Z. Wang, Y. Huan, P.Y. Zhao, X.M. Liu, T. Wei, Q.W. Zhang, X.H. Wang, Optimizing the grain size and grain boundary morphology of (K,Na) NbO_3-based ceramics: paving the way for ultrahigh energy storage capacitors, J. Materiomics. 7 (2021) 780–789, https://doi.org/10.1016/j.jmat.2020.12.009.
[60] Z. Yu, J.T. Zeng, L.Y. Zheng, A. Rousseau, G.R. Li, A. Kassiba, Microstructure effects on the energy storage density in $BiFeO_3$-based ferroelectric ceramics, Ceram. Int. 47 (2021) 12735–12741, https://doi.org/10.1016/j.ceramint.2021.01.133.
[61] H.Y. Zhou, X.Q. Liu, X.L. Zhu, X.M. Chen, $CaTiO_3$ linear dielectric ceramics with greatly enhanced dielectric strength and energy storage density, J. Am. Ceram. Soc. 101 (2018) 1999–2008, https://doi.org/10.1111/jace.15371.
[62] Y.J. Wu, Y.H. Huang, N. Wang, J. Li, M.S. Fu, X.M. Chen, Effects of phase constitution and microstructure on energy storage properties of barium strontium titanate ceramics, J. Eur. Ceram. Soc. 37 (2017) 2099–2104, https://doi.org/10.1016/j.jeurceramsoc.2016.12.052.
[63] Y.H. Huang, Y.J. Wu, W.J. Qiu, J. Li, X.M. Chen, Enhanced energy storage density of $Ba_{0.4}Sr_{0.6}TiO_3$-MgO composite prepared by spark plasma sintering, J. Eur. Ceram. Soc. 35 (2015) 1469–1476, https://doi.org/10.1016/j.jeurceramsoc.2014.11.022.
[64] H. Takahashi, Y. Numamoto, J. Tani, K. Matsuta, J.H. Qiu, S. Tsurekawa, Lead-free barium titanate ceramics with large piezoelectric constant fabricated by microwave sintering, Jpn. J. Appl. Phys. 45 (2006) L30–L32, https://doi.org/10.1143/JJAP.45.L30.
[65] Z. Song, S.J. Zhang, H.X. Liu, H. Hao, M.H. Cao, Q. Li, Q. Wang, Z.H. Yao, Z.J. Wang, M.T. Lanagan, Improved energy storage properties accompanied by enhanced interface polarization in annealed microwave-sintered BST, J. Am. Ceram. Soc. 98 (2015) 3212–3222, https://doi.org/10.1111/jace.13741.
[66] Y.P. Pu, L. Zhang, Y.F. Cui, M. Chen, High energy storage density and optical transparency of microwave sintered homogeneous $(Na_{0.5}Bi_{0.5})_{(1-x)}Ba_xTi_{(1-y)}Sn_yO_3$ ceramics, ACS Sustain. Chem. Eng. 6 (2018) 6102–6109, https://doi.org/10.1021/acssuschemeng.7b04754.
[67] J.X. Ding, Y.F. Liu, Y.N. Lu, H. Qian, H. Gao, H. Chen, C.J. Ma, Enhanced energy-storage properties of $0.89Bi_{0.5}Na_{0.5}TiO_3$-$0.06BaTiO_3$-$0.05K_{0.5}Na_{0.5}NbO_3$ lead-free anti-ferroelectric ceramics by two-step sintering method, Mater. Lett. 114 (2014) 107–110, https://doi.org/10.1016/j.matlet.2013.09.103.
[68] P.Y. Zhao, H.X. Wang, L.W. Wu, L.L. Chen, Z.M. Cai, L.T. Li, X.H. Wang, High-performance relaxor ferroelectric materials for energy storage applications, Adv. Energy Mater. 9 (2019) 1803048, https://doi.org/10.1002/aenm.201803048.
[69] F. Yan, H.R. Bai, G.L. Ge, J.F. Lin, C. Shi, K. Zhu, B. Shen, J.W. Zhai, S.J. Zhang, Composition and structure optimized $BiFeO_3$-$SrTiO_3$ lead-free ceramics with ultrahigh energy storage performance, Small 18 (2022) 2106515, https://doi.org/10.1002/smll.202106515.
[70] I.W. Chen, X.H. Wang, Sintering dense nanocrystalline ceramics without final-stage grain growth, Nature 404 (2000) 168–171, https://doi.org/10.1038/35004548.
[71] Q.Z. Chai, D. Yang, X.M. Zhao, X.L. Chao, Z.P. Yang, Lead-free (K,Na)NbO_3-based ceramics with high optical transparency and large energy storage ability, J. Am. Ceram. Soc. 101 (2018) 2321–2329, https://doi.org/10.1111/jace.15392.
[72] Y. Song, M. Zhang, S. Lan, B.B. Yang, Y.Q. Liu, C.W. Nan, Y.H. Lin, High-temperature $BaTiO_3$-based ceramic capacitors by entropy engineering design, J. Adv. Ceram. 13 (2024) 1498–1504, https://doi.org/10.26599/JAC.2024.9220964.
[73] X.F. Su, B.C. Riggs, M. Tomozawa, J.K. Nelson, D.B. Chrisey, Preparation of $BaTiO_3$/low melting glass core-shell nanoparticles for energy storage capacitor applications, J. Mater. Chem. A 2 (2014) 18087–18096, https://doi.org/10.1039/C4TA04282D.
[74] X.F. Zhou, H. Qi, Z.N. Yan, G.L. Xue, H. Luo, D. Zhang, Large energy density with excellent stability in fine-grained $(Bi_{0.5}Na_{0.5})TiO_3$-based lead-free ceramics, J. Eur. Ceram. Soc. 39 (2019) 4053–4059, https://doi.org/10.1016/j.jeurceramsoc.2019.05.056.
[75] F. Li, L. Jin, Z. Xu, S.J. Zhang, Electrostrictive effect in ferroelectrics: an alternative approach to improve piezoelectricity, Appl. Phys. Rev. 1 (2014) 011103, https://doi.org/10.1063/1.4861260.
[76] W.F. Bai, X.Y. Zhao, Y.Q. Ding, L.J. Wang, P. Zheng, J.G. Hao, J.W. Zhai, Giant field-induced strain with low hysteresis and boosted energy storage performance under low electric field in $(Bi_{0.5}Na_{0.5})TiO_3$-based grain orientation-controlled ceramics, Adv. Electron. Mater. 6 (2020) 2000332, https://doi.org/10.1002/aelm.202000332.
[77] Z.G. Chen, F. Chang, G.G. Luo, L. Ma, J. Chen, J.E. Pei, Z.Y. Cen, Q. Feng, F. Toyohisa, N.N. Luo, Preparation and energy storage properties of <001>-textured $NaNbO_3$-based ceramics, J. Adv. Dielectr. 13 (2023) 2341001, https://doi.org/10.1142/S2010135X23410011.
[78] C. Ji, G. Chen, J. Wang, X. Bai, Z.X. Zhang, C. Chen, W. Cai, R.L. Gao, X.L. Deng, C.L. Fu, Superior energy storage performance of <001>-oriented NBT-BY-STO relaxor ferroelectric textured ceramics, J. Eur. Ceram. Soc. 43 (2023) 957–965, https://doi.org/10.1016/j.jeurceramsoc.2022.11.007.
[79] G. Chen, X. Bai, C. Ji, Z.J. Zhou, Z.X. Zhang, C. Chen, Z.T. Su, W. Cai, R.L. Gao, C.L. Fu, Synergistic effect to improve energy storage performance in <111> textured BNT-based ceramics under low electric field via orientation engineering as well as co-doping BY and STO, Mater. Res. Bull. 180 (2024) 113065, https://doi.org/10.1016/j.materresbull.2024.113065.
[80] J. Wang, Z.H. Shen, R.L. Liu, Y. Shen, L.Q. Chen, H.X. Liu, C.W. Nan, Texture engineering modulating electromechanical breakdown in multilayer ceramic capacitors, Adv. Sci. 10 (2023) 2300320, https://doi.org/10.1002/advs.202300320.
[81] M.Z. Yang, H.Y. Li, J. Wang, W.X. Shi, Q.H. Zhang, H.Z. Xing, W.B. Ren, B.Z. Sun, M.F. Guo, E.R. Xu, N.N. Sun, L. Zhou, Y. Xiao, M.F. Zhang, Z. Li, J.Y. Pan, J.Y. Jiang, Z.H. Shen, X.Y. Li, L. Gu, C.W. Nan, X. Wang, Y. Shen, Roll-to-roll fabricated polymer composites filled with subnanosheets exhibiting high energy density and cyclic stability at 200 °C, Nat. Energy 9 (2024) 143–153, https://doi.org/10.1038/s41560-023-01416-3.
[82] J.L. Qi, M.H. Zhang, Y.Y. Chen, Z.X. Luo, P.Y. Zhao, H. Su, J. Wang, H.Y. Wang, L.T. Yang, H. Pan, S. Lan, Z.H. Shen, D. Yi, Y.H. Lin, High-entropy assisted $BaTiO_3$-based ceramic capacitors for energy storage, Cell. Rep. Phys. Sci. 3 (2022) 101110, https://doi.org/10.1016/j.xcrp.2022.101110.
[83] J.M. Liu, Y. Jiang, W.C. Zhang, X. Cheng, P.Y. Zhao, Y.C. Zhen, Y.N. Hao, L.M. Guo, K. Bi, X.H. Wang, Ferroelectric tungsten bronze-based ceramics with high-energy storage performance via weakly coupled relaxor design and grain boundary optimization, Nat. Commun. 15 (2024) 8651, https://doi.org/10.1038/s41467-024-52934-x.
[84] X. Xiong, H. Liu, J. Zhang, L.L. da Silva, Z.H. Sheng, Y.H. Yao, G. Wang, M. Hinterstein, S.J. Zhang, J. Chen, Ultrahigh energy-storage in dual-phase relaxor ferroelectric ceramics, Adv. Mater. 36 (2024) 2410088, https://doi.org/10.1002/adma.202410088.
[85] J.L. Qi, M.H. Cao, J.P. Heath, J.S. Dean, H. Hao, Z.H. Yao, Z.Y. Yu, H.X. Liu, Improved breakdown strength and energy storage density of a Ce doped strontium titanate core by silica shell coating, J. Mater. Chem. C 6 (2018) 9130–9139, https://doi.org/10.1039/C8TC03181A.
[86] G. Wang, J.L. Li, X. Zhang, Z.M. Fan, F. Yang, A. Feteira, D. Zhou, D.C. Sinclair, T. Ma, X.L. Tan, D.W. Wang, I.M. Reaney, Ultrahigh energy storage density lead-free multilayers by controlled electrical homogeneity, Energy Environ. Sci. 12 (2019) 582–588, https://doi.org/10.1039/C8EE03287D.
[87] L. Zhang, Y.P. Pu, M. Chen, G. Liu, Antiferroelectric-like properties in MgO-modified $0.775Na_{0.5}Bi_{0.5}TiO_3$-$0.225BaSnO_3$ ceramics for high power energy storage, J. Eur. Ceram. Soc. 38 (2018) 5388–5395, https://doi.org/10.1016/j.jeurceramsoc.2018.08.010.
[88] J. Wang, Y. Rao, X.H. Fan, J. Zhang, L. Zhao, K.J. Zhu, Synergic modulation of over-stoichiometrical MnO_2 and SiO_2-coated particles on the energy storage properties of silver niobate-based ceramics, Ceram. Int. 47 (2021) 19595–19604, https://doi.org/10.1016/j.ceramint.2021.03.297.
[89] X.H. Fan, J. Wang, H. Yuan, L. Chen, L. Zhao, K.J. Zhu, Synergic enhancement of energy storage density and efficiency in MnO_2-doped $AgNbO_3$@SiO_2 ceramics via A/B-site substitutions, Acs Appl. Mater. Int. 14 (2022) 7052–7062, https://doi.org/10.1021/acsami.1c25234.
[90] H.Y. Wang, M.H. Cao, R. Huang, C. Tao, W.G. Pan, H. Hao, Z.H. Yao, H.X. Liu, Preparation of $BaTiO_3$@NiO core-shell nanoparticles with antiferroelectric-like characteristic and high energy storage capability, J. Eur. Ceram. Soc. 41 (2021) 4129–4137, https://doi.org/10.1016/j.jeurceramsoc.2021.02.042.
[91] C.Q. Zhu, A.Y. Li, X.H. Li, S.H. Li, Z.P. Feng, Z.M. Cai, P.Z. Feng, X.H. Wang, Ultra-stable dielectric properties and enhanced energy storage density of BNT-NN-based ceramics via precise core-shell structure controlling, J. Alloys Compd. 1010 (2025) 177556, https://doi.org/10.1016/j.jallcom.2024.177556.
[92] Y. Huan, X.Z. Wang, Y.M. Zheng, X.J. Wang, T. Wei, J. Ouyang, X.H. Wang, Achieving excellent energy storage reliability and endurance via mechanical performance optimization strategy in engineered ceramics with core-shell grain structure, J. Materiomics. 8 (2022) 601–610, https://doi.org/10.1016/j.jmat.2021.11.014.
[93] L.W. Wu, G.T. Lan, Z.M. Cai, L.H. Zhao, J. Lu, X.H. Wang, Concurrent achievement of giant energy density and ultrahigh efficiency in antiferroelectric ceramics via core-shell structure design, Appl. Phys. Lett. 120 (2022) 172902, https://doi.org/10.1063/5.0088282.
[94] Q.B. Yuan, F.Z. Yao, S.D. Cheng, L.X. Wang, Y.F. Wang, S.B. Mi, Q. Wang, X.H. Wang, H. Wang, Bioinspired hierarchically structured all-inorganic nanocomposites with significantly improved capacitive performance, Adv. Funct. Mater. 30 (2020) 2000191, https://doi.org/10.1002/adfm.202000191.

[95] X.T. Zhang, L.L. Zhao, Y. Qiu, Y. Wang, Y.Y. Fan, X.R. Liu, B. Cui, Achieving comprehensive temperature-stable energy storage properties in core-shell $Na_{0.4}K_{0.1}Bi_{0.5}TiO_3$@($SrZrO_3$-$BiMg_{0.5}Sn_{0.5}O_3$)@$SiO_2$ ceramics via a multi-scale synergistic optimization, Chem. Eng. J. 462 (2023) 142251, https://doi.org/10.1016/j.cej.2023.142251.

[96] W. Huang, Y. Chen, X. Li, G.S. Wang, J.K. Xia, X.L. Dong, Superior energy storage performances achieved in (Ba, Sr)TiO_3-based bulk ceramics through composition design and Core-shell structure engineering, Chem. Eng. J. 444 (2022) 135523, https://doi.org/10.1016/j.cej.2022.135523.

[97] X.Y. Dong, X. Li, X.L. Chen, Z. Tan, J.G. Wu, J.G. Zhu, H.F. Zhou, (1-x)[0.90NN-0.10Bi($Mg_{2/3}Nb_{1/3}$)O_3]-x($Bi_{0.5}Na_{0.5}$)$_{0.7}Sr_{0.3}TiO_3$ ceramics with core-shell structures: a pathway for simultaneously achieving high polarization and breakdown strength, Nano Energy 101 (2022) 107577, https://doi.org/10.1016/j.nanoen.2022.107577.

[98] H.T. Li, X. Li, Y.X. Du, X.X. Chen, H.L. Qin, Y. Tabak, A. Evcin, F. Hussain, K.X. Song, H.F. Zhou, J.W. Zhao, D.W. Wang, Remarkable energy storage performance of $BiFeO_3$-based high-entropy lead-free ceramics and multilayers, Chem. Eng. J. 499 (2024) 156112, https://doi.org/10.1016/j.cej.2024.156112.

[99] P.T. Yang, K. Sun, Q. Hou, H.Y. Zheng, R.H. Fan, Sandwich-structured $BaTiO_3$/Ag ceramics embedded with a negative-epsilon layer to obtain high permittivity and suppress dielectric loss, J. Eur. Ceram. Soc. 44 (2024) 2173–2181, https://doi.org/10.1016/j.jeurceramsoc.2023.11.027.

[100] F. Yan, H.B. Yang, L. Ying, T. Wang, Enhanced energy storage properties of a novel lead-free ceramic with a multilayer structure, J. Mater. Chem. C 6 (29) (2018) 7905–7912, https://doi.org/10.1039/C8TC02368A.

[101] F. Yan, H.R. Bai, X.F. Zhou, G.L. Ge, G.H. Li, B. Shen, J.W. Zhai, Realizing superior energy storage properties in lead-free ceramics via a macro-structure design strategy, J. Mater. Chem. A 8 (2020) 11656–11664, https://doi.org/10.1039/D0TA03526B.

[102] G.X. Jin, J.G. Chen, J.R. Cheng, Investigation of the (1-x)($Bi_{0.85}La_{0.15}$)FeO_3-x$PbTiO_3$ multilayered ceramics by tape casting, Ceram. Int. 41 (2015) S314–S318, https://doi.org/10.1016/j.ceramint.2015.03.173.

[103] S. Chao, F. Dogan, $BaTiO_3$-$SrTiO_3$ layered dielectrics for energy storage, Mater. Lett. 65 (2011) 978–981, https://doi.org/10.1016/j.matlet.2010.12.043.

[104] J.Y. Miao, Y. Wu, Z.Q. Zhang, F.Q. Zhang, Z.F. Liu, Y.X. Li, Dielectric behavior of ($Ba_{0.95}Ca_{0.05}$) ($Zr_{-0.15}Ti_{0.842}Mg_{0.008}$)$O_3$-($Ba_{0.95}Ca_{0.05}$)($Zr_{0.08}Ti_{0.92}$)$O_3$ layered ceramics, Ferroelectrics 492 (2016) 17–24, https://doi.org/10.1080/00150193.2015.1072029.

[105] P.Y. Zhao, Z.M. Cai, L.L. Chen, L.W. Wu, Y. Huan, L.M. Guo, L.T. Li, H. Wang, X.H. Wang, Ultra-high energy storage performance in lead-free multilayer ceramic capacitors via a multiscale optimization strategy, Energy Environ. Sci. 13 (2020) 4882–4890, https://doi.org/10.1039/D0EE03094E.